الجمهورية الجزائرية الديمقراطية الشعبية	
People's Democratic Republic of Algeria	
وزارة التعليم العالي و البحث العلمي	
Ministry of Higher Education and Scientific Research	
جامعة عبد الحميد بن باديس – مستغانم	
Abdel Hamid Ibn Badis University – Mostaganem	
كلية العلوم و التكنولوجيا	
Faculty of Sciences and Technology	
قسم الهندسة الميكانيكية	
Department of Mechanical Engineering	

Registration number N°: M2...../GM/2025

END-OF-STUDIES THESIS ACADEMIC MASTER'S DEGREE

Field: Mechanical Engineering

Specialization: Energy

Topic

Numerical and Thermal analysis of Turbulent Flow around an Electronic Component

Presented by:

BEKKADOUR Benatia Mahmoud and KHACEF Abdesselam

Defended on 29/06/2025 before the jury composed of:

President:	GUERMAT Abdelkader	Maitre de Conférences "B"	University of Mostaganem UMAB
Examiner:	SAHRAOUI Nassim	Maitre de Conférences "B"	University of Mostaganem UMAB
Supervisor:	ATTOU Youcef	Maitre de Conférences "B"	University of Mostaganem UMAB

Academic year: 2024 - 2025

Dedication

With deep love and sincerity, I dedicate my finale project

To dearest mother and kindest father may you find in this work a source of pride and joy

To my sibiling who supported me throughout this path

To myself , the one who never gave up despite all the Obstacles

this is only the beginning of a bright future, God willing

To my future wife, this is a token of love and dedication for you
To everyone who truly loves me

With all my heart

Mahmoud

I dedicate this work
To my dear parents for their love, support, and sacrifices
To my brothers and my sister
To all my family
To all my friends
To all my teachers who have supported me throughout my journey.

Abdesselam

Acknowledgements

First and foremost, we thank ***Allah***, the Almighty and Most Merciful, for granting us the health, patience, and strength necessary to successfully complete this work. Without His will and blessing, nothing would have been possible.

We would like to express our deepest gratitude to **our parents** for their invaluable love, constant sacrifices, and unwavering support throughout our journey. Their trust and prayers have been our source of inspiration and motivation.

Our sincere thanks also go to our supervisor, **Dr. *Attou Youcef***, for his availability, insightful advice, kind guidance, and the quality of his supervision throughout this thesis. His scientific rigor and attentive support have been of great help to us.

We would also like to extend our heartfelt appreciation to the members of the jury:

Dr. Germat Abdelkader, president of the jury, for his insightful remarks and valuable feedback

Dr.Sahraoui Nassim, jury member, for his constructive suggestion and generous support

We sinserely thank all our professors for their and support throughout our academic journey

We also thank everyone who contributed, directly or indirectly, to our success.

List of figures

List of tables

Nomenclature

T	Temperature, [K]
U_{in}	Inlet velocity of fluid, [m.s-1]
U_j	**Jet velocity**, [$m.s^{-1}$]
C_p	Heat capacity at constant pressure, [J kg^{-1} K^{-1}]
S_x , S_z	Length and width of the cavity, [m]
H	Height of the cavity and the cylinder, [m]
p	Depth of the V shape, [m]
D	Jet diameter, [m]
P	Pressure, [Pa]
Re	Reynolds number
ρ	Fluid density, [kg/m3]
λ	Thermal conductivity, [W.m-1. K-1]
ν	Kinematic viscosity, [m2.s-1]
ε	Turbulence dissipation rate, [m2.s-3]
ν_t	Turbulent kinematic viscosity, [m2.s-1]
ω	Specific dissipation rate, [s-1]

Abstract

This numerical study examines how V-shaped groove modifications improve turbulent airflow and heat transfer around a 75°C electronic component using computational fluid dynamics simulations with ANSYS Fluent and SST turbulence model validation. Two groove configurations (internal and external) were tested systematically at different depths (P=0.05-0.2) and Reynolds numbers (Rej=1705-5115, Re_{in} =3410-8880). External V-shaped grooves with maximum depth (P=0.2) better than regular and internal configurations in terms of heat dissipation, enhanced convective mechanisms, improved flow mixing, and reduced thermal wake formation, establishing outside geometric modifications as efficient solutions for high-performance electronic thermal management applications.

Key words: Electronic cooling, V-shaped grooves, CFD, turbulent flow, Reynolds number, SST model

Résumé

Cette recherche numérique analyse l'amélioration de l'écoulement d'air turbulent et du transfert thermique autour d'un dispositif électronique à 75°C grâce à des modifications de rainures en forme de V, en utilisant des simulations de dynamique des fluides numériques avec ANSYS Fluent et la validation du modèle SST. Deux configurations de rainures (interne et externe) ont été constamment examinées en fonction de diverses profondeurs (P=0.05-0.2) et nombres de Reynolds (Rej=1705-5115, Re_{in}=3410-8880). Les analyses indiquent que les profils externes en forme de V avec profondeur maximale (P=0.2) présentent une meilleure performance thermique, atteignant une dissipation de chaleur optimale grâce à des procédés convectifs optimisés, un flux amélioré et une réduction du sillage thermique par rapport aux configurations internes et régulières, prouvant l'efficacité des adaptations géométriques externes pour les applications thermiques de haute performance.

Mots-clés : Refroidissement électronique, rainures en forme de V, CFD, écoulement turbulent, nombre de Reynolds, modèle SST

الملخص

تتناول هذه الدراسة العددية تحسين التدفق الهوائي المضطرب ونقل الحرارة حول مكون إلكتروني بدرجة حرارة 75°م باستخدام تعديلات الأخاديد على شكل V من خلال محاكاة ديناميكا الموائع الحاسوبية مع ANSYS Fluent ونموذج الاضطراب .SST تم تقييم تكوينين للأخاديد (داخلي وخارجي) بصورة منهجية عبر أعماق مختلفة (P=0.05-0.2) وأرقام رينولدز .(Rej=1705-5115, Re_{in}=3410-8880) تظهر النتائج أن الأخاديد الخارجية على شكل V بأقصى عمق (P=0.2)توفر أداءً حرارياً متفوقاً، محققة تبديد حراري مثالي من خلال آليات حمل محسنة، وخلط تدفق محسن، وتشكيل أثر حراري مخفض مقارنة بالتكوينات العادية والداخلية، مما يؤسس التعديلات الهندسية الخارجية كحلول فعالة لتطبيقات الإدارة الحرارية الإلكترونية عالية الأداء.

الكلمات المفتاحية :التبريد الإلكتروني، أخاديد على شكلV ، ديناميكا الموائع الحاسوبية ، التدفق المضطرب، رقم رينولد، نموذجSST

Table of contents

General Introduction

For many decades, the study of turbulent flows with heat transfer has been fundamental to scientific research due to its applications in a wide range of technological sectors such as electronic cooling systems, heat exchangers, and aircraft. The complex behavior of turbulent flow around 3D objects, such as electronic components, makes modeling and heat prediction extremely challenging.

With the ongoing miniaturization of electronic devices and the increase in power density, thermal constraints are becoming increasingly critical. Insufficient heat dissipation can lead to excessive temperature rise, thereby reducing the reliability, performance, and lifespan of components. According to several studies, poor thermal management is now one of the main causes of failure in electron circuits

In this context, the numerical analysis of the thermal and flow behavior around an electronic component has become essential in thermal design. Numerical simulations make it possible to study, at a lower cost, different cooling configurations and conditions, while offering a detailed view of the temperature field and flow structures.

The work is divided into four primary segments. The first chapter discusses the study into cooling methods for electronic components, with an emphasis on turbulent flows. The second chapter focuses on modeling physical processes such the Navier-Stokes equations, convection concepts, and turbulence models. The third chapter discusses the numerical methods used, namely the finite volume approach and the fluent software. Finally, the fourth chapter analyzes and assesses the collected data, with an emphasis on the effect of various geometries on thermal behavior surrounding the component. A detailed conclusion highlights the work's contributions and suggests areas for additional exploration

Chapter I:

General Overview of electronic component & State of the art

I.1 Introduction

Electronic components must be cooled in order to perform properly and last as long as possible. Indeed, these components generate heat during operation, owing primarily to the resistance in their circuits. If this heat is not efficiently dissipated, it can degrade performance, damage components, and even cause system failures.

Several techniques are used to ensure this cooling, such as natural convection, forced convection, immersion cooling, or micro-channel cooling. The choice of method depends on the amount of heat to be dissipated, as well as physical constraints such as available space, cost, or system complexity.

Processors, graphic cards, power supply units, and hard drives are all components that require proper thermal dissipation. Manufacturers frequently provide specific recommendations to increase cooling, such as the use of heat sinks, fans, or thermal pastes to improve heat flow between components and dissipators.

I.2 Heat transfer

Heat transfer is a critical activity in many industrial and technological fields since it is commonly required to manage the temperature of machinery, equipment, and industrial processes in order to ensure proper and safe operation. Radiation, conduction, and convection are the three most frequent methods of heat transfer. However, convection is the most common

form of heat transfer in many industrial applications, especially for cooling processors, electronic components, radiators, and heat exchangers.

I.2.1 Heat transfer modes

Heat transfer can occur through three different mechanisms: conduction, convection, and radiation.

- Conduction

Conduction is a type of transfer that results from molecular and atomic "collisions." It is a spontaneous energy transfer on a small scale, within a body that is locally at rest. It can occur in solids and, to a lesser extent, in fluids. Materials are classified as conductors or insulators of heat [1]. Fourier's Law was established experimentally by Joseph Fourier in 1822. This law states that the rate of heat transfer through a material is proportional to the negative temperature gradient and the area perpendicular to this gradient through which heat flows [2]

$$\Phi = -\lambda . S . \frac{dT}{dx} \qquad (I.1)$$

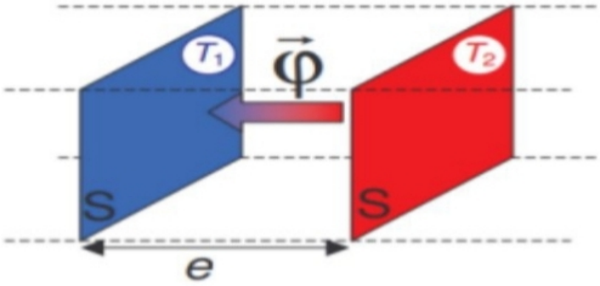

Figure I.1: Heat transfer between two surfaces (T2 > T1).

• Convection:

Convection is a type of heat transmission that occurs when the heat-carrying material moves in bulk. As a result, convection occurs in fluids (whether gasses or liquids). It is frequently seen in heat exchange at the interface of a solid and a fluid. It is critical to distinguish between forced convection, in which the fluid is propelled by an external mechanical energy source (such as a

pump, fan, etc.), natural convection, in which the fluid generates the energy required for movement from within itself, and mixed convection, which combines both mechanisms [1].Newton's law, as shown in the equation below, defines the link between the heat flux exchanged between the surface and the fluid and the exchange surface area.

$$\Phi = h.\ S.\ (Ts - Tf) \qquad (I.2)$$

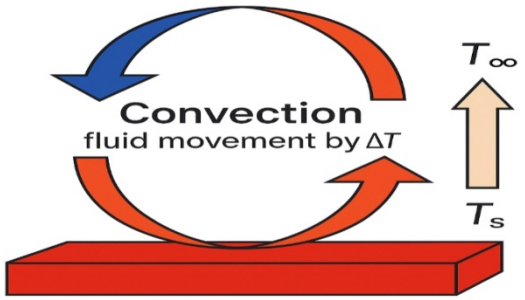

Figure I.2: Diagram of the heattransfer phenomenon by convection.

➢ Radiation:

Heat transfer by radiation is the transport of energy due to the emission of electromagnetic waves or photons from a surface or a volume. It does not Does not require a heat transfer fluid and can occur in a vacuum. This mode of transfer is described by Stefan's law [5]

$$\Phi = \mathcal{E}.\ \delta.A.\ T4 \qquad (I.3)$$

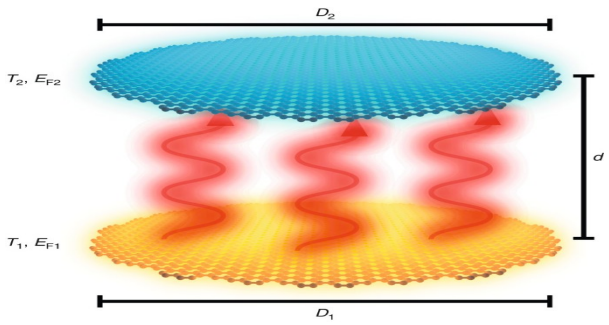

Figure I.3: Ultrafast radiative heat transfer

I.3 Thermal Aspects of Electronic Components

I.3.1 Thermal Characteristics

- Semiconductor Components

Semiconductors are materials whose conductivity is somewhere between that of conductors (metals) and insulators (most ceramics). They can be made from pure elements or compounds, and their operating temperature range is limited by the semiconductor material's characteristics and the manufacturing process used [6].

These components are often housed in hermetically sealed packaging such as TO5, TO36, flat ceramic, and plastic containers. A considerable portion of the energy supplied is converted into heat at the junction, which is primarily dissipated via conduction through the die, the die-to-package interface, and eventually the package itself [7].

- Cylindrical Tubes

Operation of electronic tubes is based on the thermo-electronic effect, also known as the thermionic effect. These are glass tubes from which the air has been evacuated, thus creating a vacuum. They consist of electrodes designed to regulate the flow of electrons between the electrodes sealed inside the vacuum tube.

Vacuum tubes primarily use thermoelectric emission, in which a metal is heated to release electrons. This process creates a positive charge on the anodes that attracts the negatively charged electrons generated by the cathodes, resulting in an electric current flow between the anode and the cathode [8].

I.4 Heating of Electronic Components

Electronic components such as integrated circuits, resistors, and capacitors are engineered to endure specified temperatures. During regular operation, they produce heat as a byproduct. However, internal or external influences can cause overheating and damage to these electronic components [9].

I.4.1 Causes of Overheating in Electronic Components

- Design and Engineering Issues

Compact high-power electronic devices and miniaturized components are particularly vulnerable to overheating due to their small size and limited dimensions, which reduce thermal transfer efficiency. In fact, the more electrons are concentrated in a small piece of semiconductor, the more they scatter phonons, preventing them from evacuating heat. Other design and engineering issues, such as faulty wiring or improper coupling, as well as a lack of quality control and evaluation during the production of electronic devices, can also contribute to overheating risks [10].

- Environmental Factors

Weather and temperature fluctuations in the surrounding environment can produce thermal stress on electrical components. Furthermore, high humidity or moisture levels in the air can taint and corrode metallic components, causing short circuits.

Other causes of overheating include poor external contact and defective wiring, which can lead to excessive voltage surges and power dissipation. Incorrect use of an electronic device such as using incompatible auxiliary devices (poorly synchronized cables and power adapters, over clocking computer components, improper storage, or excessive use) can also be an aggravating factor [9].

I.4.2 Effects of Overheating in Electronic Components

Damage to an electronic component is a direct result of overheating. Exposure to excessive temperatures can cause fatigue failure in conductive materials, such as copper.

Among the other consequences of exposure to excessive heat are the evaporation of metals or the deterioration of materials used for soldering or bonding the various parts of a component or an electronic assembly. These effects demonstrate how overheating leads to changes in the physical and chemical properties of components.

As a result, this causes material degradation and ultimately the failure of the electronic component. These alterations affect performance, and in other words, the functioning and reliability of the component [9].

I.5 Main Cooling Techniques Used in Electronics

To solve thermal issues that can impact the operation of electronic circuits, an effective cooling system is implemented to improve reliability and prevent premature failure. When selecting a cooling method, it is essential to consider eight factors: size, cost, thermal efficiency, noise level, vibrations, ease of maintenance, and possible electrical interference with other electronic components.

I.5.1 Air Cooling

Air cooling technology is one of the most common and widely used methods. It involves using air as a heat transfer fluid, which comes into contact with a heat sink, either through forced convection (with controlled airflow) or natural convection (without forced air circulation) [11].

- Natural Air Convection

Passive air cooling is primarily based on a heat sink designed according to the surface area required for cooling. The heat generated by the component is collected by the heat sink before it is discharged into the surrounding air. This system is preferred for its thermal qualities, such as strong diffusivity and thermal capacity, particularly with materials such as copper or aluminum [11].

- Forced Air Convection

Cooling electronic components by blowing forced air using a fan is the most commonly used method due to its ease of implementation, affordable cost, and reliability. The air is set in motion by a flow generator, as illustrated in the example below [12].

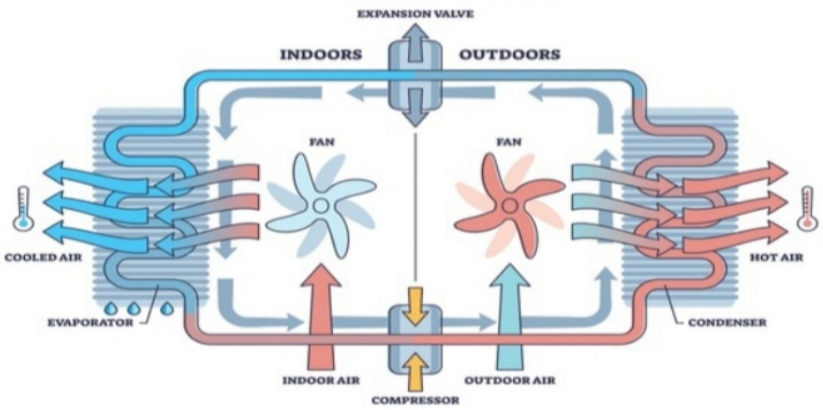

Figure I.4: Air conditioning system.

- The Piezoelectric Pump

The piezoelectric air pump, known as the "dual piezo cooling jet," is a microfluidic device composed of two nickel disks connected on either side by a piezoelectric ceramic powered by alternating current. This system, silent and motorless, stands out for its slim design and low energy consumption compared to traditional fans [12].

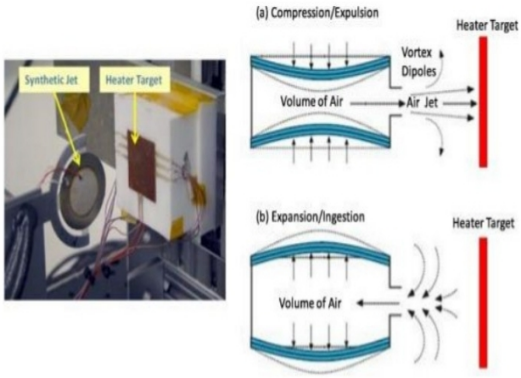

Figure I.5: The piezoelectric pump and its operating principle.

I.5.2 Cooling with Heat Transfer Liquid

The value of the convective heat transfer coefficient h is limited in the case of air due to its low thermal conductivity. To improve this coefficient and thus increase the dissipated power, it is possible to replace air with another fluid. In many cases, water is used because of its high

thermal conductivity and ease of use. In other situations, dielectric fluids such as Fluorinert, Midel, or R12 may also be employed [13]

- Water Plate Cooling

Liquid cooling is implemented in electronic components in the form of a water plate through which a heat transfer fluid circulates or channels a wall fluid to be cooled. The system mainly consists of a pump and a heat exchanger immersed in a liquid that transfers heat to the outside of the server [14].

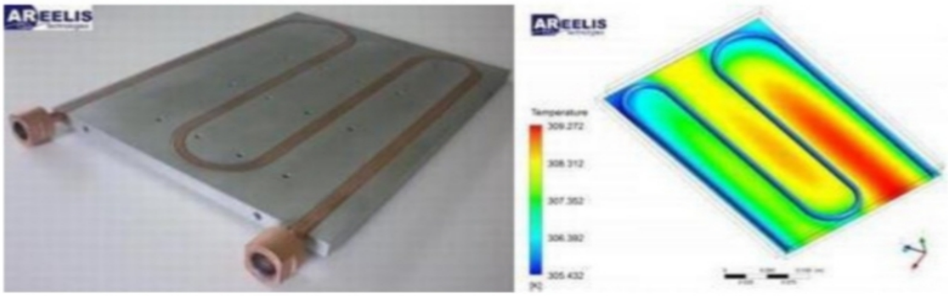

Figure I.6: Liquid cooling with cold plate.

- Cooling by Channels

Cooling using miniature or microscopic channels is a particularly interesting solution for thermal management of power electronics. Indeed, this technique makes it possible to dissipate heat flux densities that can reach several hundred W/cm². Mini and microchannels can take on more or less complex shapes, depending on the desired thermal effect and the manufacturing technology used. The simplest configuration consists of parallel rectangular channels arranged axially [15].

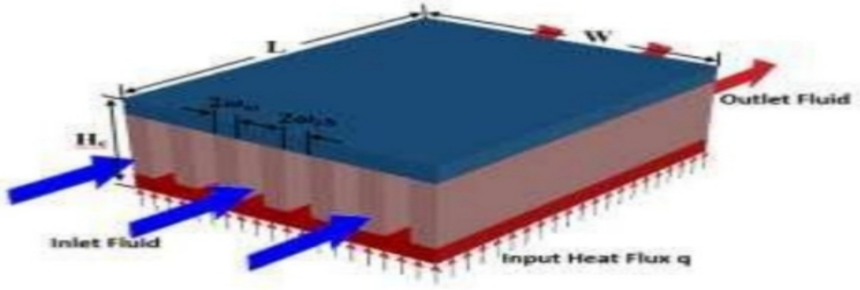

Figure I.7: Convection cooling in channels.

I.5.3 Jet cooling

Water jet cooling is a popular choice for industrial applications that need to remove huge amounts of heat from material surfaces. This technology is commonly used in the aerospace industry, namely to cool turbine blades and combustion chambers in next-generation engines.

In the electronics industry, the increasing power dissipation of current components, along with downsizing limitations, necessitates the use of efficient heat extraction systems in constrained environments [16].

I.5.4 Heat Pipe Cooling

The heat pipe is a two-phase cooling system that uses the phase change of a heat transfer fluid to carry heat from one point to another without the need for pumps or mechanical equipment. It is composed of a hermetically sealed tube with fluid-filled capillaries along the inner walls. It has three components: the evaporator, the condenser, and the adiabatic zone.

This system is distinguished by its ultra-high thermal conductivity, semi-isothermal operation, and precise temperature control [17].

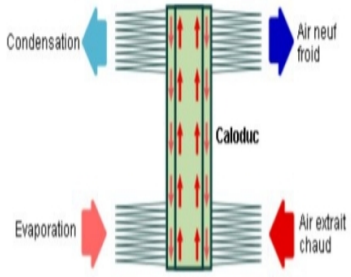

Figure I.8: Operating principal of a heat pipe.

I.6 State of the Art

Numerous scientific studies have been devoted to the analysis of electronic component cooling by convection, in its three forms (natural, forced, and mixed). Among these studies is the work of Castro and Robins [18], who used Hot Wire Anemometry (HWA) in an experimental

approach to measure the velocity field around an isolated cube placed on a flat plate. They observed that the size of the recirculation zone located behind the cube, in the region of the wake, as well as that of the vortex forming above the cube, strongly depends on the inlet flow conditions and its upstream development.

Other experimental studies were conducted by Hussein and Martinuzzi [19], Larousse et al. [20], and Martinuzzi and Tropea [21]. These studies aimed to analyze the flow around a single cube placed in a multi-layer wind tunnel generating a turbulent flow.

These works provide a detailed description of the flow, particularly through the study of the Reynolds number, calculated based on the cube height and the bulk velocity, with a value of

Re = 40,000. Figure I.9 illustrates the different types of vortices formed around the cube.

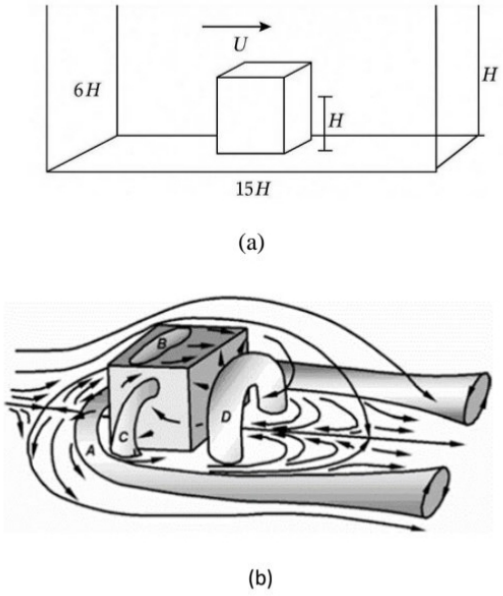

Figure I.9: Representative diagram: a) Geometry and dimensions of the computational domain b) Different types of vortices around the cube

Natural convection experiments focused on the cooling of blocks simulating electronic components were conducted by Moffat and Ortega [22]. These blocks were arranged on one of the two parallel vertical walls, with a layout of 80 blocks distributed in 8 columns and 10 rows (see Figure I.10). The experimental results showed that the fluid flow adjacent to the blocks

corresponds to forced convection, even when the fluid motion is driven by buoyancy. When the Gr/Re^2 ratio is less than 0.3, the value of the heat transfer coefficient remains within a 5% margin compared to that obtained during forced convection tests. Here, Re represents the Reynolds number, calculated from the upstream flow velocity in the channel and the height of the block B, and Gr is the local Grashof number.

Furthermore, Ortega and Moffat [23] conducted additional experimental simulations on the cooling of electronic components. They studied natural air convection for cooling an arrangement of 10 rows and 8 columns of heated aluminum cubes mounted on a plate, with and without interlocking of the cubes (see Figure I.10).

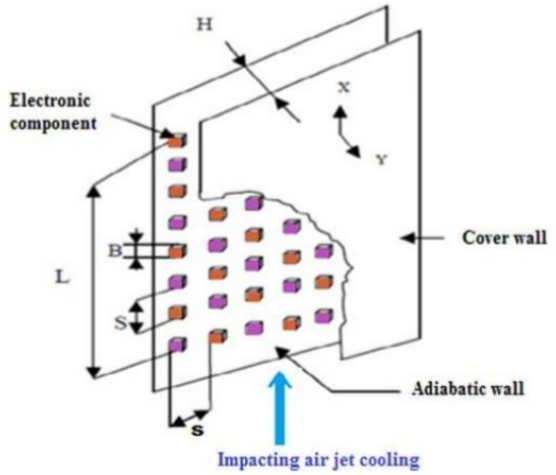

Figure I.10: Arrangement of electronic components in the channel

Youn and Vafai [24] investigated two-dimensional forced convection cooling with heat sources placed on the channel's bottom wall (Figure I.11). Their research investigates the influence of a number of factors, including the height and breadth of the sources. Furthermore, the normalized thermal conductivity ratio (ks/kf) is used,where ks represents the heat source's thermal conductivity and kf represents the fluid's. They also investigated the impact of the Reynolds number on heat transmission. The findings highlight the importance of the geometry and thermal properties of the source materials in determining flow characteristics and heat transfer performance.

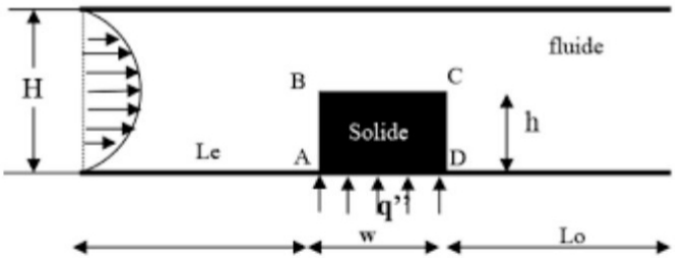

Figure I.11: Channel containing a single heated obstacle

Kim et al. [25] studied the forced pulsating flow and the associated heat transfer characteristics in a channel containing two heated blocks (see Figure I.12). At the channel inlet, the fluid has a constant temperature Tc and is driven by a velocity U, where U_0 represents the average velocity over a cycle, A is the amplitude of the axial velocity oscillations at the inlet, ω is the angular frequency, and τ is time. The blocks are maintained at a constant temperature Th. The results showed that the fluid circulation, particularly in the regions downstream of and between the blocks, is strongly influenced by the Reynolds number, the Strouhal number (St), the pulsation amplitude, as well as the spacing between the blocks.

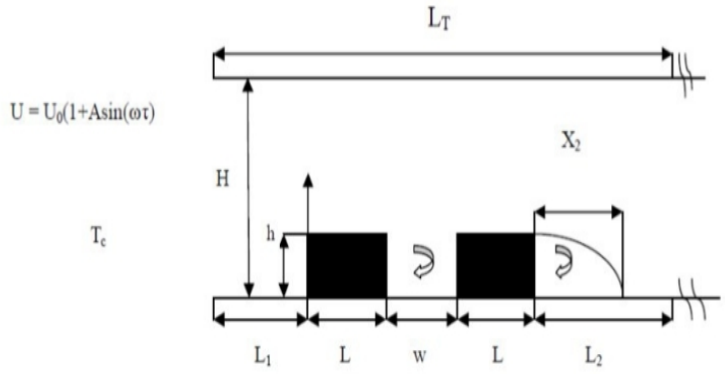

Figure I.12: Horizontal channel containing heated blocks under pulsating flow.

Kim and Anand [26] performed a numerical analysis on two-dimensional forced convection in the laminar regime within channels with five evenly heated blocks attached to one wall and slots (see Figure I.13). They investigated the effects of the Reynolds number, block height, and slot size and location on cooling performance, which was assessed using the Nusselt number (Nu) and block temperatures. Three configurations regarding the position of the slots were examined:

slots located on the left (case 1), in the center (case 2), and on the right (case 3) of the cavity. The objective of this approach is to optimize cooling without increasing the power required for thermal pumping. Comparative studies found that the blocks with slots performed significantly better in terms of cooling than the reference design without slots. This benefit became more obvious as the slot size increased. Among the conditions studied, case 3 exhibited the greatest increase in the Nusselt number, while case 2 showed the smallest.

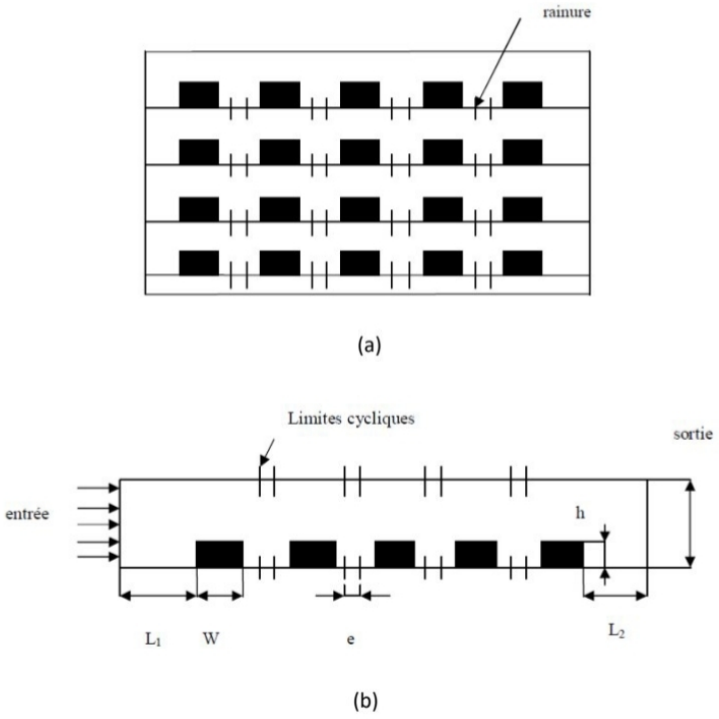

Figure I.13: Model of a Two-Dimensional Channel with Slots
(a) Two-Dimensional Channels
(b) Computational Domain of a Two-Dimensional Channel with Slots

Icoz and Jaluria [27] developed a methodology for the design and optimization of cooling systems for electronic equipment. Two simple configurations were used to demonstrate this approach (Figure I.14).

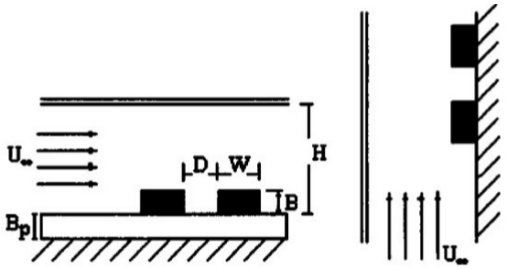

Figure I.14: Horizontal and vertical channels containing electronic components.

Hamouche and Bessaih [28] simulated laminar mixed convection in a horizontal channel with both ends open (Figure I.15), with two identical heat sources representing electronic components. The study investigated how the Reynolds number, component separation distance, and dimensions (height and width) influenced flow patterns and heat transfer inside the channel. Correlations were used to get the average Nusselt number for both components. The results revealed a considerable increase in heat transmission for Reynolds numbers ranging from 5 to 30. Furthermore, it was discovered that increasing the separation distance, height, and breadth of the components significantly enhances heat dissipation, thereby improving cooling performance. This improvement was more noticeable in the second component than in the first.

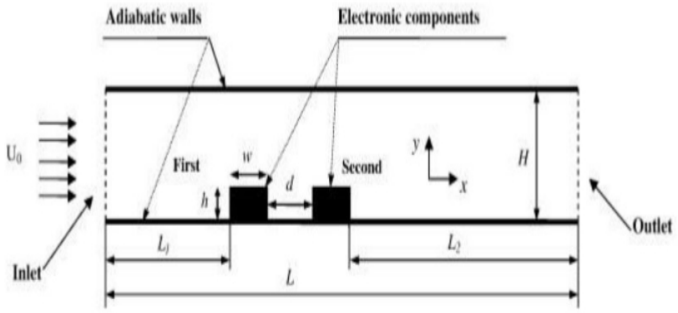

Figure I.15: Geometry of the problem.

Amirouche Y. and Bessaih R. [29] numerically studied turbulent natural convection for the cooling of five electronic components arranged along a wall in a vertical channel. The simulation results, compared with experimental data, revealed that the channel width and the absence of heating in certain components significantly influence the enhancement of heat transfer within the channel (see Figure I.16).

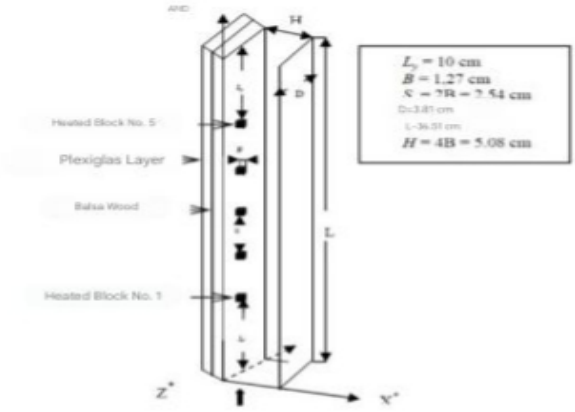

Figure I.16: Five cubic heat sources, simulating electronic components, mounted on a vertical wall of a channel.

Niceno et al. [30] conducted a numerical study of flow dynamics and heat transfer through an array of heated cubes attached to a wall of a flat channel (see Figure I.17), a configuration representative of electronic component cooling. Using Large Eddy Simulation (LES), they determined the temperature field inside the cube and on its outer surface, which served as boundary conditions for convection. The results showed that the local heat transfer between the cube and the fluid strongly depends on the coherence of vortex structures in the immediate vicinity of the cube. The frontal impact of the flow and its separation at the sharp edges of the cube enhance heat transfer, while recirculation zones reduce cooling efficiency. The highest temperatures were observed on the rear face of the cube, forming a characteristic thermal arc. Furthermore, a persistent vortex develops in the wake region, increasing the residence time of the fluid in that area. The temperature distribution on the cube's surface was in very good agreement with experimental results.

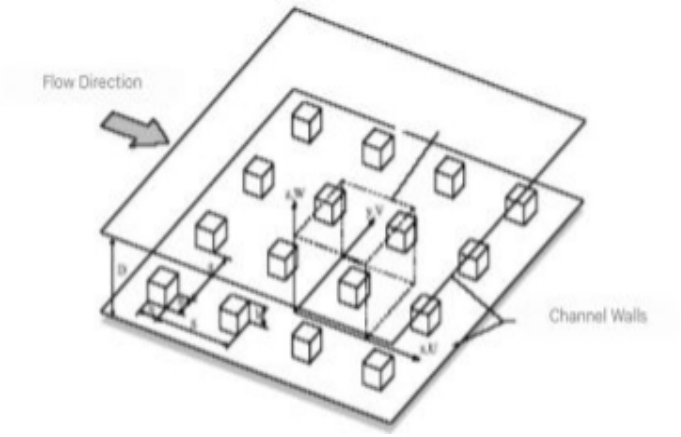

Figure I.17: Configuration of the cube matrix.

Meinders E.R. and Hanjalić K. [31] studied the structure of turbulent flow as well as the distribution of the heat transfer coefficient on the surfaces of a cube placed within a matrix of cubes located in a flat channel. To do this, they used infrared thermography to measure the temperature on the cube's walls, which enabled them to determine the local distribution of the heat transfer coefficient. The flow structure was analyzed using laser Doppler anemometry (LDA) and flow visualizations. Their results revealed that the flow formed vortical structures only near the walls of the cube, while above the cube and in the longitudinal corridors, the flow was mainly swirling, with high turbulence intensity. The flow separation on the top and side faces of the cube induced recirculations and flow reattachment near these surfaces. This reattachment of the shear layer to the bottom wall of the channel generated a two-cell structure in the region between the obstacles: a hairpin vortex downstream of the cube and a horseshoe vortex upstream at the base of the cube.

Flow instabilities caused the periodic detachment of vortices along the sidewalls of the cube, resulting in periodic motions in the wake region. The analysis of the Strouhal number revealed a constant value of St = 0.109. The flow structure particularly the separation and reattachment phenomena—directly influences the local distribution of the heat transfer coefficient, with significant gradients observed on the top and side walls of the cube (see Figure I.18).

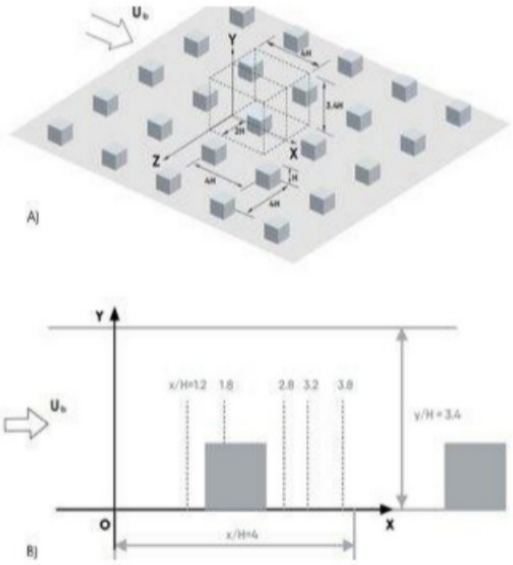

Figure I.18: Three-dimensional diagram representing the configuration of the cube matrix in a channel (top view) and the configuration of the sub-domain (bottom view).

Several cooling solutions have been developed with the purpose of optimizing heat transmission and improving heat dissipation. The most common cooling systems rely on natural and forced convection using gaseous or liquid fluids. Natural convection works well in low-power systems and situations with low heat flow density. For high-power or large-scale systems with strict heat dissipation requirements, forced convection is considered the most effective and widely used method. Sakakibara et al. [32] conducted an experiment to evaluate the effect of vortical features on heat transfer in the stagnation zone of an impinging jet. The investigation was carried out using the Particle Image Velocimetry (PIV) technique, for a range of Reynolds numbers from 2,000 to 20,000, this range being defined based on the jet diameter. The experimental results highlighted the formation of a pair of counter-rotating vortices, accompanied by an amplification of vortical structures, which led to a notable enhancement in heat transfer in the stagnation region (see Figure I.19).

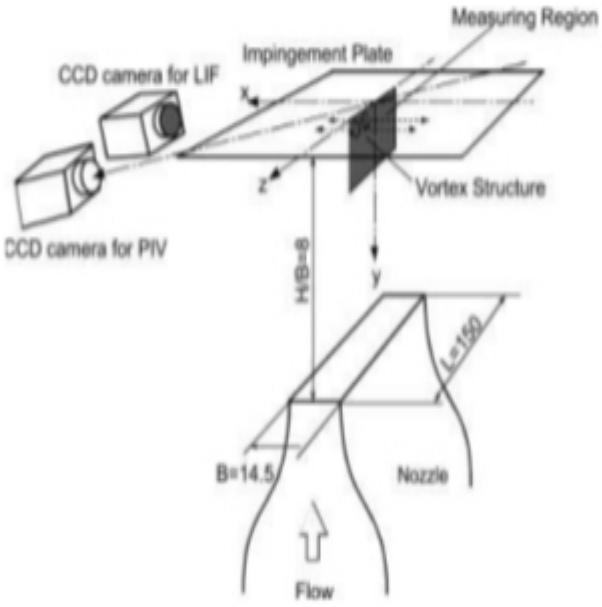

Figure I.19: Experimental setup and system coordinates.

In the following study, the geometric configuration under investigation closely resembles the one experimentally studied by Masip et al. [33]. This configuration consists of a cube heated to a temperature of 60°C, placed in a forced air flow at a temperature of 20°C. The cube is also exposed to a perpendicular jet from above, which is also at a temperature of 20°C.Masip et al. [33] studied the influence of the Reynolds numbers (Re_j and Re_H) on the flow structure. Three Reynolds numbers 3410, 5752, and 8880 were investigated, corresponding to the following ratios: 0.5, 1.0, and 1.5, respectively.

The results showed that, in the case of a low Reynolds number, the impinging jet does not reach the top surface of the cube, which eliminates the presence of the horseshoe vortex on the upper surface and alters the flow characteristics in the region above the cube.

The geometric configuration is illustrated in Figure I.20. The numerical results obtained in this study are compared with the experimental measurements of Masip et al. [33].

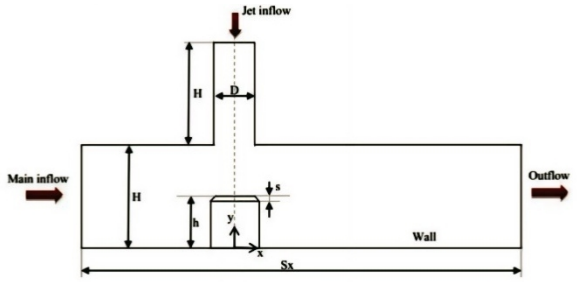

Figure I.20: Diagram representing the computational domain, boundary conditions, and local coordinate system.

Rundstrom and Moshfegh [34] carried out a numerical simulation under mixed convection to predict the turbulence characteristics of a jet flow over the heated surface of a cube (see Figure I.21). Two different simulations were conducted: Large Eddy Simulation (LES) and the Reynolds Stress Model (RSM). A comparison between the simulation results and experimental data was performed.

The results revealed that the flow structure is highly complex, involving several flow phenomena such as stagnation points, flow separation, recirculation, and curvature effects. The results showed that temperature prediction using LES is in better agreement with experimental results compared to the RSM simulation, particularly in the stagnation region.

Furthermore, the temperature length scale predictions obtained from LES were also closer to the experimental measurements on the front and rear faces of the cube compared to those predicted by RSM.

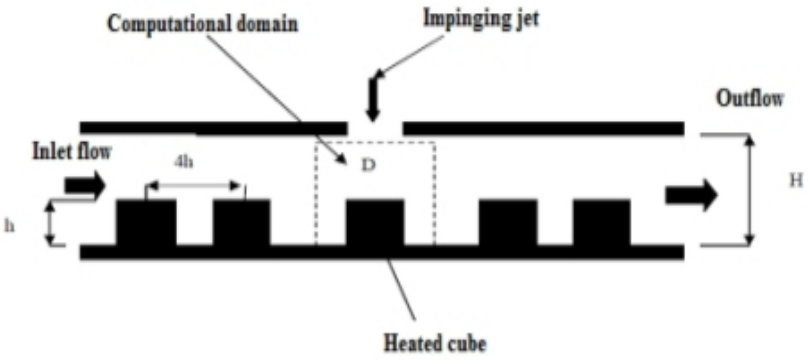

Figure I.21: Sketch diagram of the experimental setup.

Chapter II :

Modelling of Turbulence

I.7 Introduction

In this chapter, we will present the general equations governing the studied phenomenon, as well as a description of the main turbulence models, in order to select the appropriate one. The useful relationships for predicting flows are derived from the fundamental conservation laws of mass, momentum, and energy. In the most general case, the variables considered are the density ρ, the velocity components Ui, the pressure P, and the temperature T.

I.8 Turbulence Phenomenon

Turbulence refers to the state of a fluid, whether liquid or gas, in which the velocity at every point exhibits a swirling character: vortices whose size, location, and orientation constantly vary. Turbulent flows are thus characterized by a highly disordered appearance, unpredictable behavior, and the existence of many spatial and temporal scales. Such flows occur when the kinetic energy driving the fluid's motion relatively intense is compared to the viscous forces that resist movement. Conversely, a flow is called laminar when it behaves in a regular and orderly manner [46].

The discovery and study of turbulence date back to ancient times; for example, Leonardo da Vinci observed and described it. Osborne Reynolds revitalized the study of turbulence at the end of the 19th century.

The complex behavior of turbulent flows is most often approached using statistical methods. Therefore, the study of turbulence is considered part of statistical physics. To express the fact that, in a flow, inertial forces dominate over viscous forces, a properly chosen Reynolds number

must exceed a certain threshold. For the study of turbulence in natural environments, it is preferable to use the Richardson number rather than the Reynolds number, since the latter assumes constant fluid density, which is not valid in the case of compressible fluids.

I.9 Main Numerical Approaches to Turbulence

The main approaches for numerically studying turbulence are:

DNS: Direct Numerical Simulation
LES: Large Eddy Simulation
RANS: Reynolds-Averaged Navier-Stokes equations

I.9.1 Direct Numerical Simulation (DNS)

Direct Numerical Simulation (DNS) solves all spatial and temporal fluctuations without the need for modeling. However, it is extremely computationally expensive and is limited to simple geometries (Figure II.1)

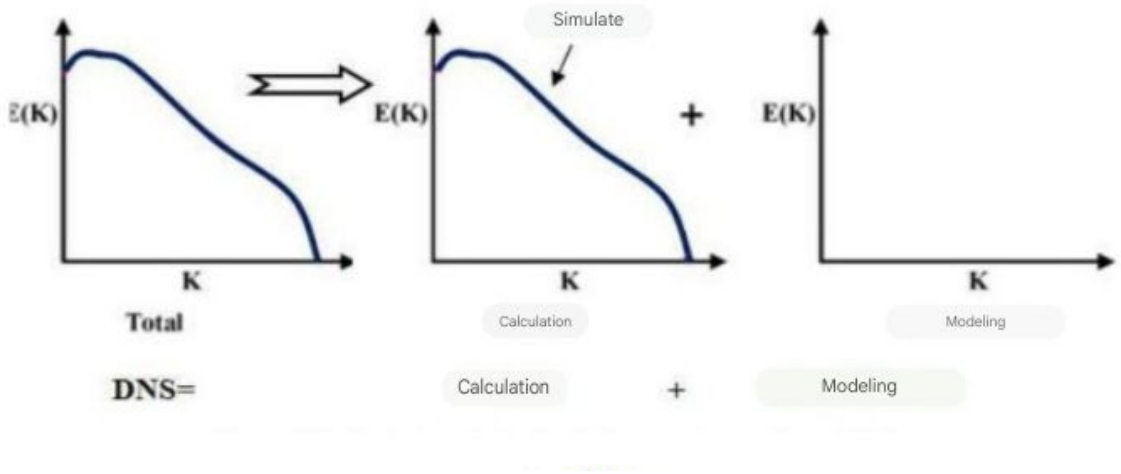

Figure II.1: Technique of direct numerical simulation (DNS)

I.9.2 Large Eddy Simulation (LES)

Large Eddy Simulation (LES) was initially proposed in the 1960s to simulate atmospheric flows. With the advancement of computational capabilities, this method has become one of the most promising and effective approaches for simulating turbulent flows, particularly complex engineering flows. This approach was first introduced in 1963 by Smagorinsky [35]. In large-scale turbulent flows, the large eddies are computed directly, while only the small-scale motions are modeled (see Fig. II.2). This strategy allows for a reduction in computational cost compared to Direct Numerical Simulation (DNS) [36]

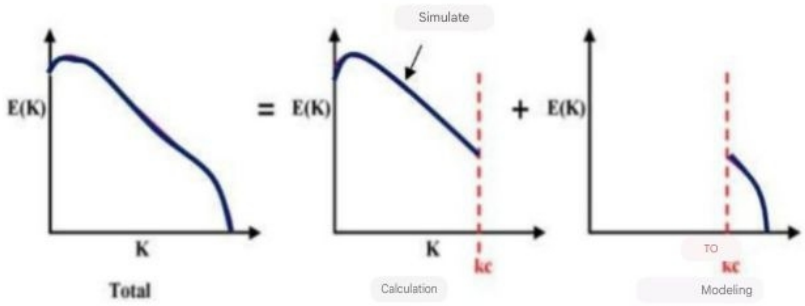

Figure II.2: Technique of Large Eddy Simulation (LES)

Large Eddy Simulation (LES) offers greater accuracy than the RANS approach because it directly captures the large vortices, which contain the majority of turbulent energy. Unlike RANS, where these structures are entirely modeled, LES resolves them explicitly, enhancing the representation of dynamic phenomena. Moreover, the small scales of turbulence, which are generally more isotropic and homogeneous than the large ones, are easier to model. This makes the LES approach more effective in faithfully reproducing turbulent behavior compared to RANS, which attempts to model all turbulence scales within a single framework.

II.3.2 Reynolds-Averaged Navier-Stokes (RANS)

The numerical resolution of the Reynolds-Averaged Navier-Stokes (RANS) equations relies on solving transport equations applied only to the mean quantities, with all turbulence scales being modeled. This approach, which resolves only the mean variables, significantly reduces

computational costs. However, due to the inherent complexity of turbulence, it is unlikely that a RANS model can accurately capture all turbulent scales. For this reason, RANS models often rely on statistical methods to handle these phenomena [37].

The RANS (Reynolds-Averaged Navier-Stokes) approach remains the most widely used method for modeling turbulent flows. To transition from the Navier-Stokes equations to the RANS equations, it is assumed that the fluctuating velocity components (turbulent) can be separated from the mean velocity. This separation of a variable into a mean component ($\overline{u}$; mean velocity) and a fluctuating component (u′) is commonly referred to as "Reynolds decomposition." Thus, the Reynolds decomposition of a velocity component (ui) is:

$$u_i(x,t) = \overline{u}_i\ (x)\ +\ u_i'(x,t) \tag{II.1}$$

In some cases, the main interest lies in the steady-state flow of the fluid, and it is not necessary to simulate the detailed instantaneous flow, which leads to a significant reduction in computation time. This is the basis of the Reynolds-averaged Navier-Stokes (RANS) approach, in which only the averaged quantities are solved, while the effects of all instantaneous turbulent motion scales are modeled using a turbulence model.

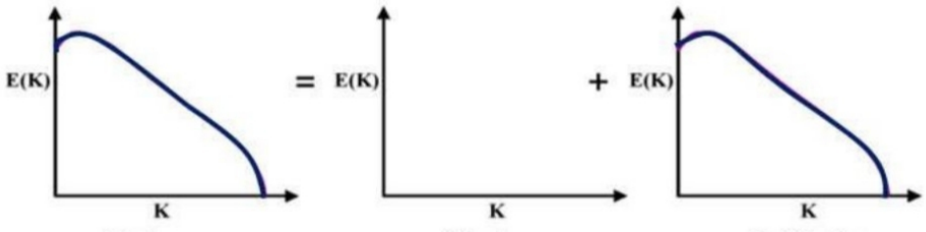

Total Calculatuion Modeling

Figure II.3: Technique of Static RANS Simulation

The approach introduced by Reynolds consists of describing instantaneous quantities as fluctuations around their mean values. The instantaneous values of velocity, pressure, and temperature are thus decomposed into mean and fluctuating components [38].

$$u = \bar{u} + u'$$

$$V = \overline{V} + V' \qquad \text{(II.2)}$$

$$\text{w} = \overline{w} + w'$$

$$P = \overline{P} + P'$$

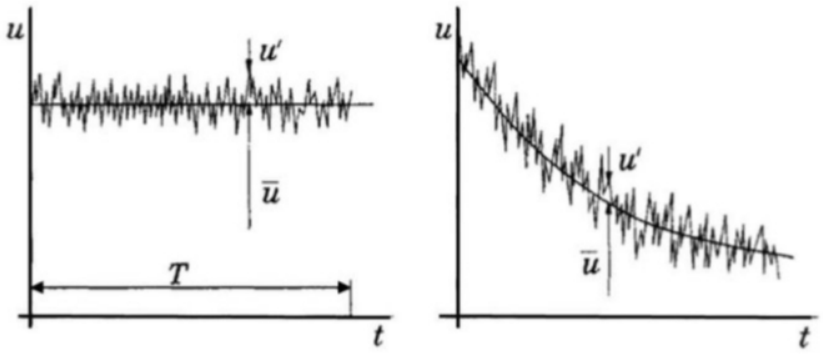

Fgure II.4: Temporal evolution of the velocity in turbulent conditions

I.10 Governing equations

The governing equations are expressed in differential form, derived by considering a fixed infinitesimal control volume. These conservation equations for mass, momentum, and energy take the form of nonlinear partial differential equations [39]. The differential analysis of fluid flow and heat transfer can only be solved numerically using a CFD code (such as ANSYS FLUENT, ANSYS CFX, Open FOAM, STAR-CCM+, etc.).

CONTINUITY EQUATION

$$\frac{\partial u_j}{\partial x_j} = 0 \qquad \text{(II.3)}$$

MOVEMENT QUANTITY EQUATION

$$\rho U_j \frac{\partial}{\partial x_j}(U_i) = -\frac{\partial P}{\partial x_j} + \mu \frac{\partial^2 u_i}{\partial x^2{}_j} + \underbrace{\frac{\partial}{\partial x_j}\left(-\rho \overline{u_i' u_j'}\right)}_{\text{Constraints of Reynolds}} + \rho g_i \tag{II.4}$$

ENERGY EQUATION

$$\frac{\partial}{\partial x_j}\left(\rho U_j T\right) = \frac{\lambda}{Cp} \frac{\partial^2 T}{\partial x^2{}_j} + \frac{\partial}{\partial x_j}\left(-\overline{\rho u_j' t_p'}\right) \tag{II.5}$$

All of these equations have the following general form:

$$\underbrace{\frac{\partial(\rho u_j \phi)}{\partial x_j}}_{1} = \underbrace{\frac{\partial}{\partial x_j}\left(\Gamma_\phi \frac{\partial \phi}{\partial x}\right)}_{2} + \underbrace{S_\phi}_{3} \tag{II.6}$$

Term 1: transport of ϕ by convection.

Term 2: transport of ϕ by diffusion.

Term 3: local production of ϕ.

I.11 Closure Models

Turbulence modeling is a research topic that has been extensively studied and has many practical applications across a wide range of industries. Since the early work of Boussinesq [40] and Prandtl in 1975, numerous models have been developed [37]. More recently, efforts have been made to develop transport models using Reynolds stress tensors that depend on anisotropy parameters and include higher-order terms for pressure correlations. These models make it possible to represent what can be considered "extreme" turbulence regimes (strong anisotropies).

To model a turbulent flow, the field of turbulence modeling essentially involves using a series of mathematical equations to describe the mixing and enhanced diffusion caused by turbulent fluctuations. Turbulence models fundamentally aim to predict unknowns (such as Reynolds stresses).

The choice of a turbulence model depends on factors such as the physics involved in the flow, the required level of accuracy, the available computational resources, and the time available for

simulation. To select the most appropriate model for a given application, it is essential to understand the capabilities and limitations of the different options [41].

ANSYS Fluent provides the following turbulence model options:

- Spalart-Allmaras model
- Models (Standard, RNG, Realizable)
- Models (Standard, SST)
- Transition SST models
- Reynolds Stress Model (RSM)
- Detached Eddy Simulation (DES) model
- Large Eddy Simulation (LES) model

I.11.1 Boussinesq Hypothesis

The underlying assumption used in all turbulent viscosity models is the Boussinesq hypothesis [40], which expresses the Reynolds stress tensor in terms of the gradient of the time-averaged velocity field

$$-\rho\overline{u'_i u'_j} = \mu_t\left(\frac{\partial u_i}{\partial x_j}+\frac{\partial u_j}{\partial x_i}\right) - \frac{2}{3}\rho k\delta_{ij} \qquad \text{(II.7)}$$

Where:

μ_t is the turbulent viscosity

k is the turbulent kinetic energy

It should be noted that the Boussinesq hypothesis assumes that the turbulent viscosity is isotropic.

I.11.2 The spalart- Allmaras Model

The model solver a transport equation or the working viable $\check{\nu}$, which is directly related to the turbulent kinematic viscosity υ_t. [42]

I.11.3 The k–ε Model

This is a two-equation model within the RANS models, which means that two transport equations must be solved: the first for the turbulent kinetic energy k, and the second for its dissipation ε.

The k–ε model is one of the most widely used turbulence models. It allows the simulation of a wide range of industrially relevant flows without modifying the model constants.

The limitations of this model include weak shear layers, boundary layer separation, flows over

I.11.3.1 The Standard k–ε Model

The standard k–ε model is based on solving the transport equations of turbulent kinetic energy k and its dissipation rate ε. It assumes a fully turbulent flow, where the effects of molecular viscosity are considered negligible.

The turbulent kinetic energy k and its dissipation rate ε are determined from the following transport equations:

$$\frac{\partial(\rho k)}{\partial t} + \frac{\partial(\rho U_j k)}{\partial x_j} = P_K - \rho\varepsilon + \frac{\partial}{\partial x_j}\left(\Gamma_k \frac{\partial k}{\partial x_j}\right) \tag{II.8}$$

And

$$\frac{\partial(\rho\varepsilon)}{\partial t} + \frac{\partial(\rho U_j \varepsilon)}{\partial x_j} = C_{\varepsilon 1}\frac{\varepsilon}{k}P_k - C_{\varepsilon 2}\rho\frac{\varepsilon^2}{k} + \frac{\partial}{\partial x_j}\left(\Gamma_\varepsilon \frac{\partial k}{\partial x_j}\right) \tag{II.10}$$

With the model constants $C\varepsilon_1; C\varepsilon_2; \sigma_k; \sigma_\varepsilon$

$$\Gamma_k = \mu + \frac{\mu_t}{\sigma_k} \; ; \qquad \Gamma_\varepsilon = \mu + \frac{\mu_t}{\sigma_\varepsilon} \tag{II.11}$$

In these equations,P_k represents the production of turbulent kinetic energy due to the mean velocity gradirnt :

$$P_K = \mu_t\left(\frac{\partial U_i}{\partial X_j} + \frac{\partial U_j}{\partial X_i}\right)\frac{\partial U_i}{\partial X_j} + \frac{2}{3} + \rho k\delta_i\frac{\partial U_J}{\partial xi} \quad \text{(II.12)}$$

- Turbulent viscosity

The turbulent viscosity μ_t is calculated by combining k and ε as follows:

$$\mu_t = C_\mu \rho\frac{k^2}{\varepsilon} \quad \text{(II.13)}$$

C_μ is a model constant. The Reynolds stresses are calculated using the Boussinesq approximation

$$\rho\overline{u_i u_j} = -\mu_t\left(\frac{\partial U_i}{\partial x_j} + \frac{\partial U_j}{\partial x_i}\right) + \frac{2}{3}\rho k\delta_{i\,j} \quad \text{(II.14)}$$

- Model Constants :

The model constants, determined from experimental studies on turbulence,are as follows:

constants	$C_{\varepsilon 1}$	$C_{\varepsilon 2}$	$C_{\varepsilon 3}$	$C_{\varepsilon 4}$	$C_{\varepsilon 5}$
values	1.44	1.92	0.09	1.0	1.3

Table II.1: Constants o the standard k- ε model

I.11.3.2 The k-ε RNG Model

The k-ε RNG model (Renormalization Group Theory) is an improved version of the standard k-ε model. It offers the advantage of not requiring special treatment in near-wall regions, as it is applicable in areas characterized by low Reynolds numbers.

The transport equations for turbulent kinetic energy and dissipation rate retain the same form as those of the standard model.

$$\frac{\partial(\rho k)}{\partial t} + \nabla(\rho U\varepsilon) = \nabla\left(\mu + \frac{\mu_t}{\sigma_k}\nabla k\right) + P_k - \rho\varepsilon \quad \text{(II.15)}$$

$$\frac{\partial(\rho\varepsilon)}{\partial t} + \nabla(\rho U\varepsilon) = \nabla\left(\mu + \frac{\mu_t}{\sigma_\varepsilon}\nabla\varepsilon\right) + \frac{\varepsilon}{k}(C_{\varepsilon 1RNG}P_K - C_{\varepsilon 2RNG}\rho\varepsilon) \quad \text{(II.16)}$$

$$C_{\varepsilon 1RNG} = 1.42 - f_n \quad ; \quad f_n = \frac{\eta\left(1-\frac{\eta}{4.38}\right)}{(1+\beta_{RNG}\eta^3)} \text{and} \quad \eta = \sqrt{\frac{P_K}{\rho C_{\mu RNG}\varepsilon}} \quad \text{(II.17)}$$

And $C_{\varepsilon 1RNG}$ and $C_{\varepsilon 2RNG}$ are constants experimentally determined for turbulent flows by patankar and spalding.

Constants	C_V	$\eta 0$	β	$\sigma_K = \sigma_\varepsilon$	$C_{\varepsilon 1RNG}$	$C_{\varepsilon 2RNG}$
Values	0.0845	4.377	0.012	0.7179	1.42	1.68

Table II.2: Constants of the K- ε RNG model

I.11.3.3 The Realizable k-ε Model

The realizable k-ε model is a modified version of the standard model, in which the transport equation for turbulent kinetic energy has been revised. One of the main limitations of the standard model is that the normal stresses can become negative in flows subjected to high mean strain rates. The realizable model overcomes this limitation by enforcing a realizability constraint on the predicted stress tensor. Accordingly, the normal components of the Reynolds stress tensor, which should theoretically remain positive, are modeled as follows:

$$\langle u'_i u'_j \rangle = \Sigma_i \langle {u'_i}^2 \rangle = \frac{2}{3}K - 2v_t \frac{\partial \langle u_i \rangle}{\partial x_j} = \frac{2}{3}K - 2C_u \frac{K^2}{\varepsilon} \frac{\partial \langle u_i \rangle}{\partial x_j} \quad \text{(II.18)}$$

When the negative term containing the coefficient becomes sufficiently large, it can lead to a negative normal stress. In the realizable model, this coefficient is defined based on the local state of the flow in order to ensure that the normal stress remains positives

I.11.4 The standard $k - \omega$ Model

The $k - \omega$ model is used to estimate the turbulent viscosity μt. The turbulent kinetic energy k and the dissipation ε are determined from the ollowing equations:

$$\frac{\partial(\rho k)}{\partial t} + \frac{\partial(\rho u_j k)}{\partial x_j} = P_K - \beta' \rho k \omega + \frac{\partial}{\partial x_j}\left(\Gamma_k \frac{\partial k}{\partial x_j}\right) \quad \text{(II.19)}$$

$$\frac{\partial(\rho \omega)}{\partial t} + \frac{\partial(\rho u_j \omega)}{\partial x_j} = \alpha \frac{\omega}{k} P_K - \beta \rho \omega^2 + \frac{\partial}{\partial x_j}\left(\Gamma_\omega \frac{\partial \omega}{\partial x_j}\right) \quad \text{(II.20)}$$

With: $\Gamma_k = \mu_t + \frac{\mu_t}{\sigma_t} \Gamma_\omega = \mu + \frac{\mu_t}{\sigma_\omega}$

Constants	β'	α	$\boldsymbol{\beta}$	$\boldsymbol{\omega_k}$	$\boldsymbol{\sigma_k}$
Values	0.09	5/9	3/40	2.0	2.0

Table II.3: Constants of the standard $k-\omega$ model

II.5.4.1The $k-\omega$ SST Model

The turbulence model chosen for this study is the Shear Stress Transport (SST) model, an adaptation of the k-ω model proposed by Wilcox [43]. Developed by Menter in 1993, the SST model combines the formulation of the k-ω model with that of the k-ε model [44], using damping functions F1 and F2.

The coefficient F1 equals 1 near the wall and becomes zero away from it. This activates the Wilcox k-ω model in the near-wall region while allowing the use of the k-ε model for the rest of the flow. The k-ω SST model is described by a set of transport equations that include terms related to the generation, effective diffusivity, and dissipation of k and ω, as well as a cross-diffusion term that combines both the k-ε and k-ω models. The transport equations of the k-ω SST model are presented as follows:

$$\frac{\partial(\rho k)}{\partial t}+\frac{\partial(\rho u_j k)}{\partial x_j}=\overline{P}-\beta^*\rho k\omega+\frac{\partial}{\partial x_j}\left(\Gamma_k\frac{\partial k}{\partial x_j}\right) \quad \text{(II.21)}$$

$$\frac{\partial(\rho\omega)}{\partial t}+\frac{\partial(\rho u_j\omega)}{\partial x_j}=\frac{\gamma}{v_t}P_K-\beta\rho\omega^2+\frac{\partial}{\partial x_j}\left(\Gamma_\omega\frac{\partial\omega}{\partial x_j}\right)+(1-F_1)2\rho\sigma\omega_2\frac{1}{\omega}\frac{\partial k}{\partial x_j}\frac{\partial\omega}{\partial x_j} \quad \text{(II.22)}$$

$$\Gamma_k=\mu+\frac{\mu_t}{\sigma_t}\quad,\quad \Gamma_\omega=\mu+\frac{\mu_t}{\sigma_{\omega c}}\quad,\quad P_K=\tau_{ij}\frac{\partial U}{\partial x_j}\quad,\quad \overline{P_K}=\min(P_K,c_1\varepsilon)$$

Constants	$\varphi k1$	$\varphi\omega1$	$\gamma1$	$\beta1$	C1	K	σ_{k2}	$\sigma_{\omega2}$	$\gamma2$	$\beta2$
Values	2.0	2.0	0.5532	0.075	10	0.41	1.0	1.168	0.4403	0.828

Table II.4: Constants of the $k-\omega$ SST model

Relaxation functions F1 and F2:

$$F1=tanh\left(arg_1^4\right) \quad \text{(II.23)}$$

$$arg_1 = min\left(max\left(\frac{\sqrt{k}}{\beta^* \omega y}; \frac{500\,v}{y^2 \omega}\right); \frac{4\rho\sigma_{\omega 2} k}{CD_{K\omega y^2}}\right) \quad \text{(II.24)}$$

$$CD_{K\omega} = \max\left(2\rho\sigma_{\omega 2}\frac{1}{\omega}\frac{\partial k}{\partial x_j}\frac{\partial \omega}{\partial x_j}\right); 1.0e^{-10} \quad \text{(II.25)}$$

$$\text{F2}=tanh\left(arg_2^2\right) \quad \text{(II.26)}$$

$$arg_2 = max\left(2\frac{\sqrt{k}}{\beta^* \omega y}; \frac{500\,v}{y^2 \omega}\right) \quad \text{(II.27)}$$

$$\tau_{ij} = \mu_t\left(\frac{\partial U_i}{\partial xj} + \frac{\partial U_j}{\partial x_j} - \frac{2}{3}\frac{\partial U_K}{\partial x_K}\right) - \frac{2}{3}\rho k \delta_i \quad \text{(II.28)}$$

I.12 Conclusion

In this chapter, we discussed concepts related to turbulence modeling, as well as the governing equations that describe fluid flow and the variations in equations implemented in the numerical solver and we have also examined the different turbulence models. The next chapter will be dedicated to the description of the numerical method used, namely the finite volume method. It will also present the physical and numerical domain, including the mesh, as well as the various boundary conditions applied.

Chapter III:

Numerical Method

I.13 Introduction

Computational Fluid Dynamics (CFD) is a branch of fluid mechanics which uses numerical methods to analyze flows. It requires a good understanding of fluid dynamics in order to correctly interpret the results. The predictions provided are generally validated by experimental data, giving them a high degree of reliability. Partial differential equations (PDEs), representing conservation laws, describe fluid motion in space and time. Prior to their numerical resolution, these equations must be discretized: the study domain is divided into small cells forming a mesh, and the equations are converted into an algebraic form suitable for calculation. This chapter presents the fundamental principles of the finite volume method, the most common discretization schemes and an introduction to the Gambit (for meshing) and Fluent (for simulation) software packages.

I.14 Numerical Resolutions

In order to obtain a numerical solution to the problem under study, it is necessary to transform the differential equations of the mathematical model, by means of a discretization process, into a system of algebraic equations more suitable for computer processing. Some of the most common discretization techniques used in flow and heat transfer problems includes:

-Finite difference method
-Finite element method
-Finite volume method.

I.14.1 Finite difference method

The principle of this method consists in discretizing the domain of definition in terms of space and time variables. The division into small volumes of the medium to be studied is both a function structure and boundary conditions. In the case of solving heat equation in any medium, each node resulting from the discretization is characterized by a discrete temperature value. The heat equation is characterized by a discrete temperature value. The heat equation is then applied to the nodes in its discrete form. The result is a system of algebraic equations algebraic equations (often made up of a large number of equations) that must be solved by computer software.

I.14.2 Finite element method

This method involves dividing the domain into small elements (triangles, quadrilaterals, etc.) and formulating the equations in weak form. It is widely used in structural mechanics, allowing great flexibility in the modeling complex geometries.

I.14.3 Finite volume method

Developed by Patankar [45], the finite volume method can be used to solve conservation equations in integral form. It is based on the division of the domain into control volumes, on which the PDEs are transformed directly into simpler algebraic equations.

I.14.3.1 Principle of the finite volume method

The technique involves two important stages:

- Meshing: this consists in dividing the domain into several regular intervals called control volumes.

- Discretization: during this stage, the equations are integrated into the control volumes.

The finite volume method is based on dividing the study domain into a finite set of sub-domains called control volumes (CV), each centered around a node where the unknown variables are evaluated. These volumes cover the entire domain without overlapping, in order to simplify the analysis. Each VC leads to a discrete equation, and their number must correspond to the number

of points to be solved, once the boundary conditions. This structure is generally based on a numerical grid that serves as the basis for mesh construction.

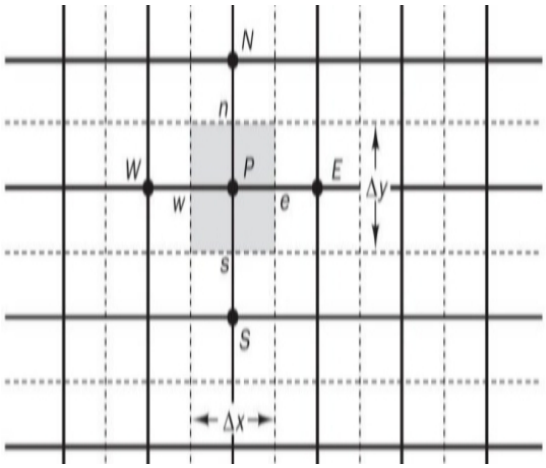

Figure III.1: Discretization of a domain into elementary volumes for a two-dimensional problem

where: P is the principal node,

i: is the discretization index along the "x" axis,

j :is the discretization index along the "y" axis.

Time is indexed by "k".

In general, the letters E, W, N and S stand for East, West, North and South respectively. and South respectively.

The gray square represents a control volume element.

The segments [PE] and [PN] are Δx and Δy respectively.

In the following, we adopt the following meshes:

→ Along the "x" axis: x(i) = (i-1)Δx

where: Δx is the discretization step along this direction.

→ Along the "y" axis: y(j) = (j-1)Δy

where : Δy is the discretization step along this direction.

The finite volume method consists in integrating the conservation equations of the various physical quantities different physical quantities:

$$\frac{\partial}{\partial t}(\rho\emptyset) + div(\rho U\emptyset) = div\left(\Gamma_{\phi} grad\emptyset\right) + S_{\emptyset} \qquad \text{(III.1)}$$

$\frac{\partial}{\partial t}(\rho\emptyset)$:Temporal term

$div(\rho U\emptyset)$:Convective term

$div(\Gamma_{\phi} grad\emptyset)$:Diffusive term

$S_{\emptyset}$:Source term

Where ∅ represents the quantity to be calculated (speed, pressure...)

Γ : indicates the diffusion coefficient

The partial differential equations are reformulated in linear form in order to can be solved using matrix methods. Each calculation node is associated with a volume on which the equations are integrated. To guarantee consistency in the exchange exchange of between nodes, neihboring control volumes must share a common face. The set of these volumes cover the entire area under study, ensuring a complete of the flow. This construction makes it possible to demonstrate the conservation of flows, particularly in the context of heat transfer.

In the specific case of axisymmetric flow and in the absence of the source term $S_{\emptyset}$ the equation can then be expressed in the following simplified form (assuming ∅=T):

$$\frac{\partial \phi}{\partial t} + \frac{\partial}{\partial x}\left[u\phi - \Gamma_{\phi}\frac{\partial \phi}{\partial y}\right] + \frac{\partial}{\partial y}\left[v\phi - \frac{\partial \phi}{\partial y}\right] = 0 \qquad \text{(III. 2)}$$

Or :

$$\frac{\partial \emptyset}{\partial t} + \frac{\partial J_x}{\partial x} + \frac{\partial J_y}{\partial y} = 0 \qquad \text{(III. 3)}$$

With :

$$J_x = \left[u\emptyset - \Gamma_{\emptyset}\frac{\partial \emptyset}{\partial x}\right] et J_y = \left[v\phi - \frac{\partial \phi}{\partial y}\right] \qquad \text{(III. 4)}$$

We'll integrate it across the control volume and with respect to time t.

$$\int_s^n \int_w^e \int_{t_1}^{t_2} \frac{\partial \emptyset}{\partial t} dt dx dy + \int_s^n \int_w^e \int_{t_1}^{t_2} \frac{\partial J_x}{\partial x} dx dy dt + \int_s^n \int_w^e \int_{t_1}^{t_2} \frac{\partial J_y}{\partial y} dy dx dt = 0 \qquad \text{(III. 5)}$$

To integrate this equation, we assume that :

- At a given time, the temperature is uniform across the control volume.
- For a given “x” or “y”, the flow is uniform along the face.
- An implicit scheme is used to ensure stability over time.

After integration, the result is :

$$\left[(\emptyset)_p - (\emptyset)_p^0\right]\Delta x\Delta y + \int_s^n (J_e - j_w)dy\Delta t + \int_w^e (j_n - j_s)dx\Delta t = 0 \quad \text{(III. 6)}$$

Or :

$$\left[(\emptyset)_p - (\emptyset)_p^0\right]\frac{\Delta V}{\Delta t} + [J_e - j_w] + [J_n - j_s] = 0 \quad \text{(III. 7)}$$

with :

$$\Delta V : Voulumesurroundingnode P\ (\Delta V = \Delta x\Delta y)$$

$$(\emptyset)_p : valueattimet + \Delta t$$

$$(\emptyset)_p^0 : value\ at\ time\ t$$

$$J_e = \int_s^n J_e dy = \left[u\phi - \Gamma_\phi \frac{\partial \phi}{\partial x}\right]_e \Delta y \quad \text{(III.8)}$$

$$J_w = \int_s^n J_w dy = \left[u\phi - \Gamma_\phi \frac{\partial \phi}{\partial x}\right]_e \Delta y \quad \text{(III.9)}$$

$$J_n = \int_w^e J_n dx = \left[v\phi - \Gamma_\phi \frac{\partial \phi}{\partial y}\right]_e \Delta x \quad \text{(III.10)}$$

$$J_s = \int_w^e J_s dx = \left[v\phi - \Gamma_\phi \frac{\partial \phi}{\partial y}\right]_e \Delta x \quad \text{(III.11)}$$

I.14.3.2 Meshing

To generate a mesh adapted to the geometry of the problem, Gambit software tetrahedral and hexahedral meshes. The tetrahedral mesh is easier to create thanks to a semi-automatic process. Hexahedral meshing, on the other hand, is more complex, requiring several steps such as defining and projecting points, curves and surfaces

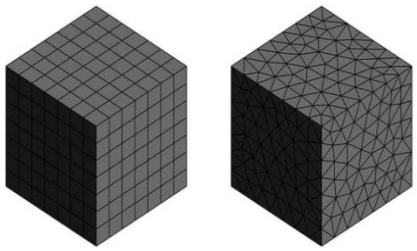

Figure III.2: hexahedral -left, tetrahedral -right

There are several types of mesh, defined by each element being associated with a certain number of node types that serve to link

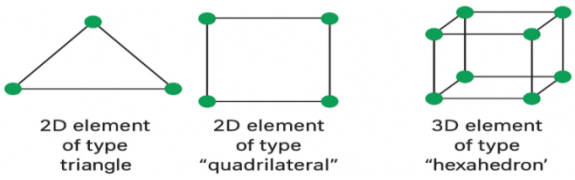

Figure III.3: Some element types

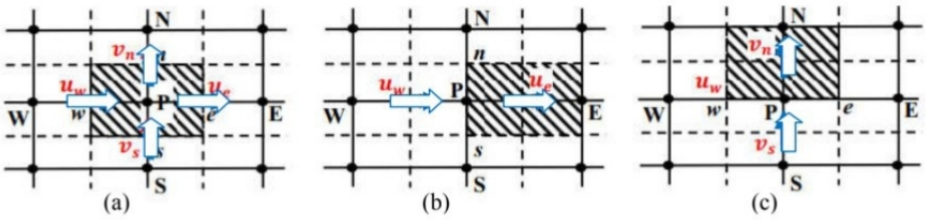

Figure III.4: (a) Mesh diagram, (b) declared mesh for u_e ,(c)declared mesh for v_n

I.14.3.2.1 Structured mesh (quadra/hexa)

Structured meshes feature regular connectivity between cells. It uses quadrilaterals in 2D and hexahedra in 3D. Thanks to its orderly organization, it offers good spatial efficiency, greater precision and faster convergence in numerical calculations.

I.14.3.2.2 Unstructured mesh (tri/tetra)

Unstructured meshes are distinguished by uneven connections between cells, making them challenging to represent as a regular array in memory. It allows for a wide range of element choices, most often triangles in 2D and tetrahedrons in 3D, making it suited for complicated designs.

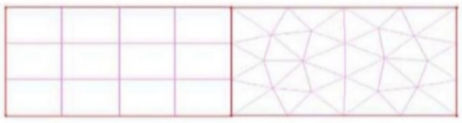

Figure III 5: The structure- left and unstructured- right

I.15 Introducing GAMBIT and FLUENT

Numerical simulations were carried out using Fluent software, based on the based on the finite volume method. The resolution procedure adopted in Fluent will be presented briefly. The geometry and mesh were constructed using using Gambit, then imported into Fluent for calculation.

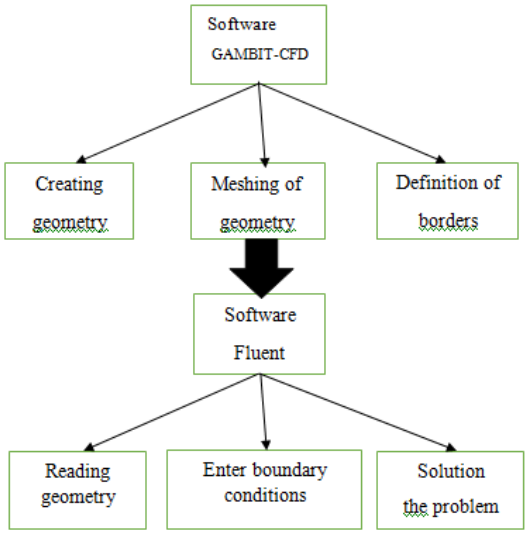

Figure III.6: Global numerical procedure for simulation using the GAMBIT CFD and FLUENT calculation codes

I.16 GAMBIT

The Gambit (Geometry And Mesh Building Intelligent Toolkit) software is a better 2D/3D pre-processor for meshing geometry domains in a CFD problem. problem. It can generate structured or unstructured meshes in Cartesian, PolarCartesian, Polar, cylindrical or axisymmetric coordinates. It can produce complex meshesin two or three Dimensions, with rectangular or triangular meshes.

Gambit's generation options offer flexibility of choice.Geometry can be broken down into several parts to generate a structured mesh. Alternatively, Gambit automatically generates an unstructured mesh adapted to the type oftype of geometry being constructed. With mesh verification tools, defects are easily detected.easily detected.It can be used to build a geometry and generate a mesh for it, if required,geometry from another CAD program can be imported into this preprocessor.It generates *.msh files for Fluent.

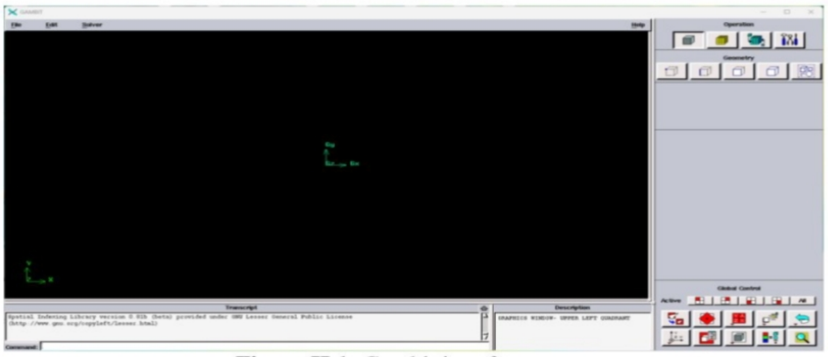

Figure III.7: Gambit interface

I.17 ANSYS Fluent

Fluent is a commercial CFD code widely used in industry. It can be used to solve fluid flow and heat transfer problems of all kinds. For example, it can calculate the lift of an aircraft wing, the drag of a car, the cooling of electronic circuits by ventilated air...etc.

When starting the Fluent software, you must select the dimensions of the calculation domain (2D or 3D), and whether the software should use single or double precision.

Figure III.8: Choice of dimensions and precision

I.17.1.1 Fluent numerical resolution procedure

After modeling the geometry and properly setting the boundary conditions, the mesh is exported, allowing the problem to be solved numerically.

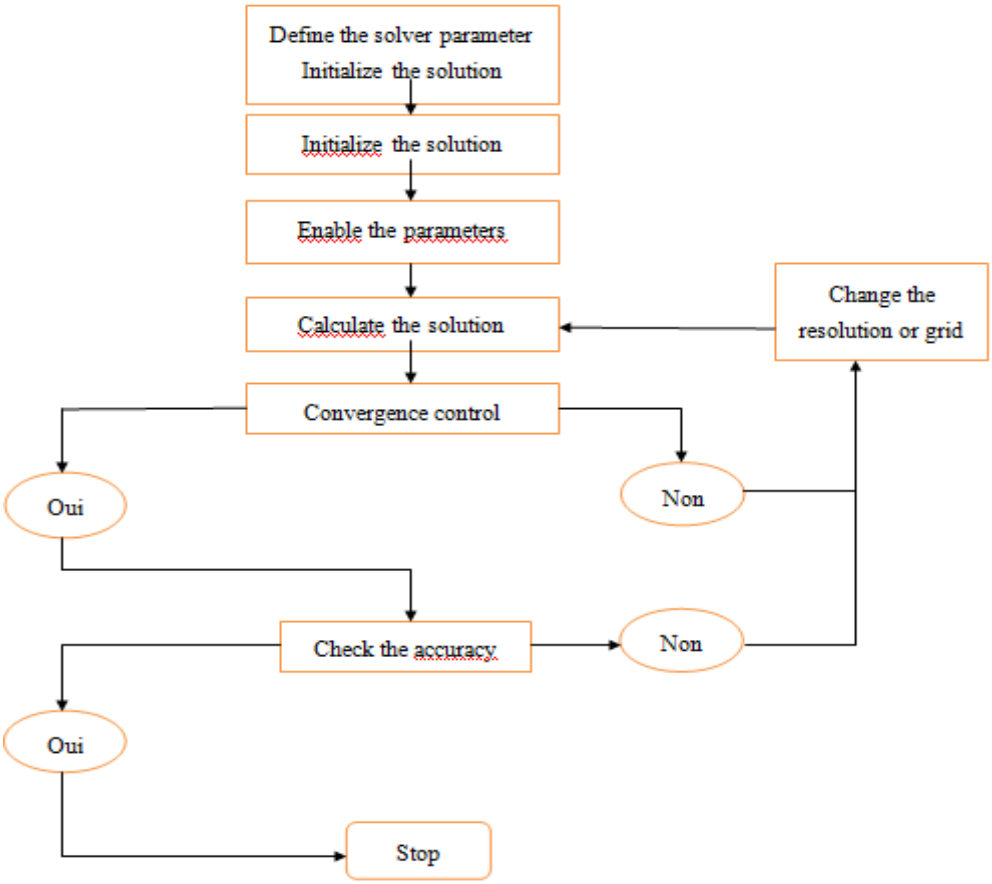

Figure III.9: Numerical solution step by FLUENT

This step is essential for discretizing the integral equations representing the fundamental conservation principles, which are mass, momentum, and energy.

I.17.1.1.1 Choice of solver formulation

There are two types of solver:

Segregated: this is the most appropriate for incompressible flows (fans,pumps...)

Coupled: the coupled implicit and coupled explicit solvers are more suitable forhigh-speed compressible flows.

This is also where the flow regime is chosen: permanent or unsteady.

Define → Models → Solver.

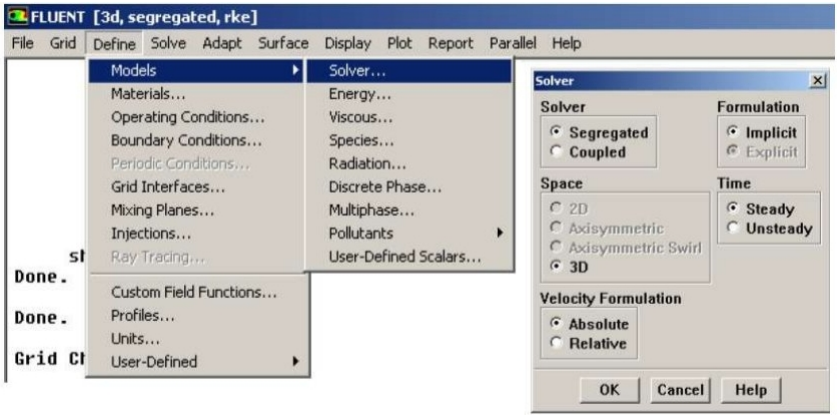

Figure III.10: Choice of fluent solver

I.17.1.1.2 Discretization scheme

In this section we present several numerical diagrams of the heat transfer phenomenon available in the "FLUENT" code. Cells be interpolated to the faces of the control volume using interpolation schemes interpolation schemes of different orders of accuracy.

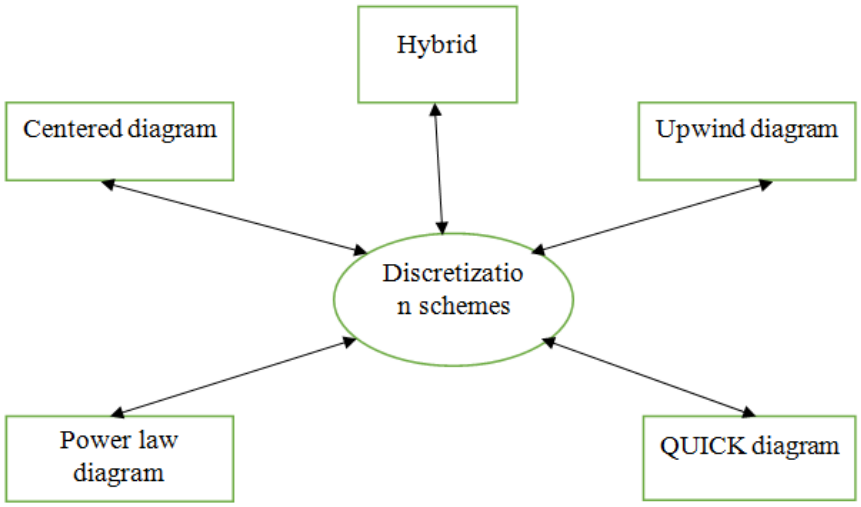

Figure III.11: Discretization schemes

The convective terms of the governing equations are discretized using these numerical schemes. Numerical schemes, and for greater accuracy the second-order scheme is automatically selected to discretize the viscous terms.

For our work, the discretization schemes used are summarized as follows:

Pressure	Standard
Energy	Second order Upwind
Quantity of motion	Second order Upwind
Velocity-pressure coupling	Simple

Table III.1: Used Discretization schemes.

I.17.1.1.3 Face pressure interpolation methods

The main methods for interpolating pressure at cell faces proposed by Fluent are:

- Standard scheme
- PRESTO diagram
- Linear diagram.
- Second-order diagram
- Body Force Weighted diagram

I.17.1.1.4 Choice of interpolation methods (Gradients)

The calculation of variable gradients is essential for the evaluation of diffusive flows, the determination of velocity derivatives, and for the application of higher-order discretization schemes. In ANSYS Fluent, these gradients are estimated gradients are estimated at mesh face level using a multi-dimensional Taylor series series. Several methods are proposed for this calculation to ensure the best possible accuracy, depending on the numerical context adopted.

$$\frac{\partial(\rho\phi)}{\partial t}V + \sum_f^{Nfaces} \rho_f V_f \emptyset_f . A_f = \sum_f^{Nfaces} \Gamma_\emptyset \nabla \emptyset_f + S_\emptyset V \qquad \text{(III.14)}$$

- Green-Gauss cell-Based
- Green-Gauss Node-Based
- Least-Squares cell-Based

I.17.1.1.5 Choice of pressure-velocity coupling method

"FLUENT" offers three methods for pressure-velocity coupling:

The two methods, very similar to each other, are the "SIMPLE" (Semi Implicit Method for a Pressure Linked Equations) method and the "SIMPLEC" (SIMPLE Consistent) method.

The latter method differs from the former in that it can be assigned a pressure relaxation correction factor close to 1. This allows for faster convergence in most cases, but can lead to solution instabilities.

The "PISO" (Pressure Implicit with Splitting of Operators) algorithm: This algorithm is part of the "SIMPLE" family of algorithms, which introduces two additional corrections instead of just one. It is recommended for non-iterative calculations of unsteady and compressible flows.

I.18 Description of the problem

This work focuses on the numerical modeling of turbulent flow around an electrical component positioned inside a rectangular channel.

The primary goal is to examine the thermal and dynamic behavior of the fluid surrounding this component in order to assess and improve cooling conditions.

The research domain consists of a channel into which a fixed barrier representing the electrical component is introduced, which can be cubic or cylindrical in shape depending on the circumstance. Air, the heat transfer fluid, flows turbulently around the impediment, resulting in recirculation zones, pressure gradients, and localized heat transfer.

The geometric dimensions, boundary limitations, and physical characteristics of the fluid are designed to mimic real-world operating conditions. After creating the mesh with GAMBIT software, the numerical solution is calculated using the finite volume method and a CFD solver (Fluent 6.3.26).

This case study investigates the implications of geometric configuration and flow conditions on system thermal performance, specifically the efficacy of cooling the electronics component.

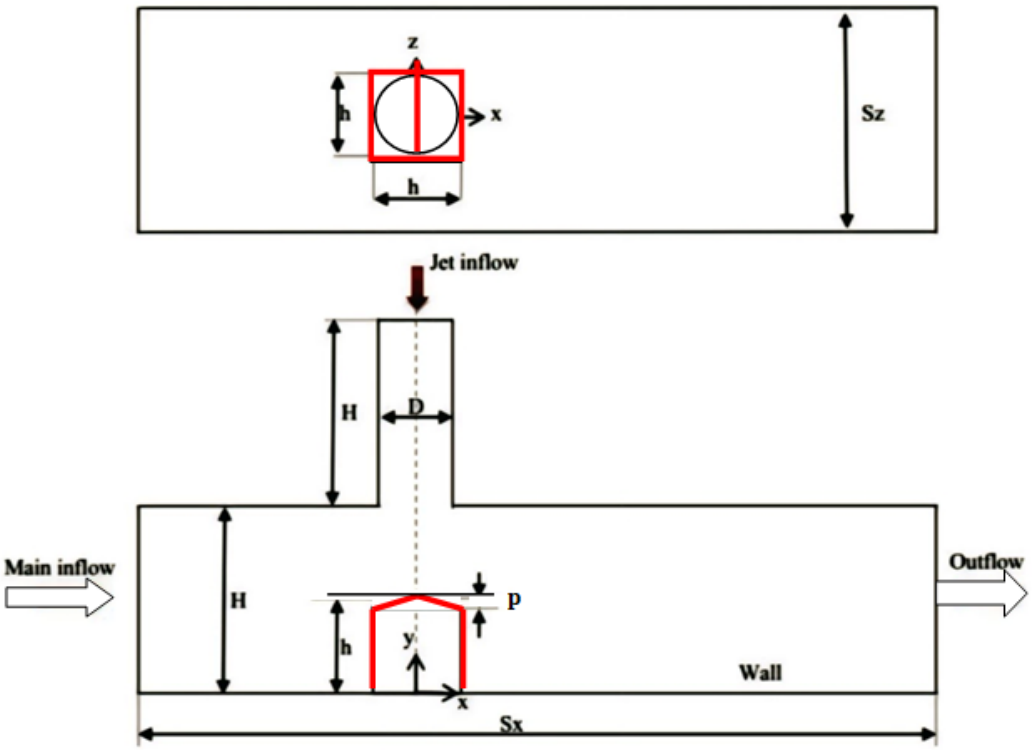

Figure III.13: Representaion of the computational domain

I.18.1 Mesh generation with GAMBIT

The mesh menu consists of five buttons as shown in the table below.

Commande	Couches limites	Segment	Faces	Volume	Groupe
Symbole					

Table III.2: Description of the mesh menu commands

The main mesh menus are described as follows:

1. Creating and modifying a boundary layer mesh
2. Setting the size of the first cell
3. Mesh expansion factor
4. Number of lines in the specific mesh

5. Mesh type (4 specific mesh types are available)

6. Meshing a line

7. Applying a double ratio that increases the density of points either on the sides or in the center of the lines

8. Using a ratio for the mesh

9. Select the mesh option: number of nodes or the size of the interval between the two

10. Face mesh

11. Smoothing of deformed meshes

12. Select the mesh type: Tri, Quad

13. If this option is checked, a regular mesh is created according to the settings below. If not,a mesh is created from the nodes defined on the edges

14. Volume mesh

15. Smoothing of deformed meshes

16. Select the mesh type: Tetra, Hex

17. If this option is checked, a regular mesh is created according to the settings below. If not, a mesh is created from the nodes defined on the edges.

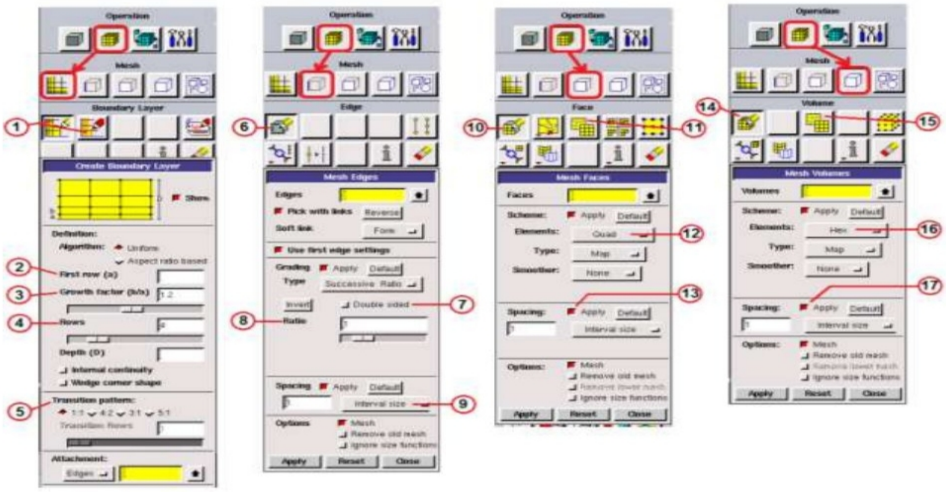

Figure III.13: Main menus of Gambit's mesh

When specifying a mesh element type, each element is associated with a scheme (Table III-3) and a mesh type (Table III-3).

Option	Description
Quad	Specifies that the mesh contains only quadrilateral elements
Tri	Specifies that the mesh contains only triangular elements
Quad / *Tri*	Spécifie que le maillage d'éléments quadrilatéraux peut contient des éléments Triangulaires

Table III.3: Specification of the face gambit element scheme

Option	Description
Map	created a mesh and structured
Submap	Divides a complex geometry face into more regular regions and creates a structured mesh in each region
Pave	creates an unstructured mesh
Tri primitive	Divide a three-sided face into three quadrilateral regions and create a structured mesh in each region

Table III.4: Specifying the mesh type of face gambit elements

I.18.2 Boundary conditions

Several types of boundary conditions are available depending on the problem being addressed. Note that the mesh space is assumed to be fluid by default. The name given to the boundary is very important because it will be used in Fluent, and if the names are unclear, the boundaries may be mixed up.

The Gambit mesh generator can generate meshes that many solvers can use, so we must specify the solver software with which we want to process the mesh file. The choice of boundary type varies depending on the solver being considered to solve the problem.

Common types of boundary conditions are:

- Inlet and jet Velocities: Used for incompressible or moderately compressible flows, when the inlet velocity is known. U_{in}=1.705m/s, U_{jet}=2.131m/s.
- Pressure Outlet : The use of this type is to define the static pressure at the outlet.

	Velocity [m/s]	**Pressure [Pa]**	**Temperature [°C]**
Inlet velocity	1.705	-	20
Jet velocity	2.131	-	20
Component	-	-	75
Outlet	-	1	20

Table III.5: Boundary conditions

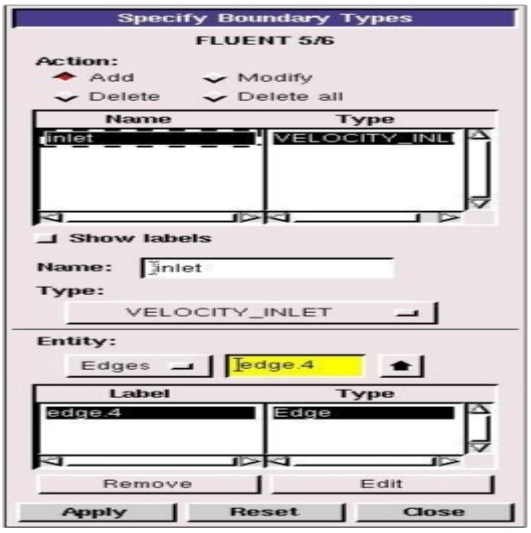

Figure III.14: main menus for boundary conditions

I.18.3 Convergence criterion

The convergence of an iterative solution is assessed primarily through residuals, according to several criteria. The residuals of the momentum, continuity, turbulence, and volume fraction equations should ideally be less than 10^{-4}However,this criterion alone does not guarantee the validity of the solution, as a solution can be correct even with large residuals, and vice versa.

The equation (III.15) defines the residual R:

$$R = \sum_{l'ensemble\ des\ volumes} |a_w \phi_w + a_E \phi_E + S_u - a_p \phi_p \quad \text{(III.15)}$$

Which tends to zero in the event of complete convergence. Graphical monitoring of the residuals allows the stability of the calculation to be assessed. Divergent residuals may indicate a problem with the mesh, formulation, or solver tuning. To resolve this, it is recommended to check the formulation, use a first-order scheme initially, and reduce the under-relaxation factors.

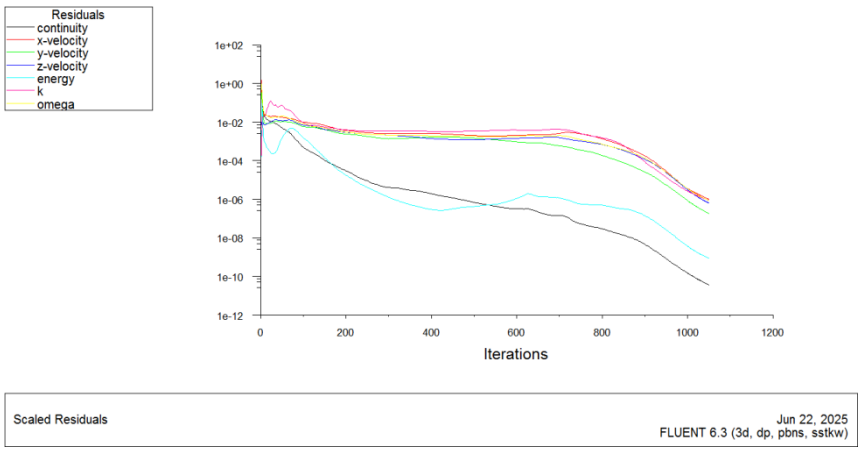

Figure III.15: Convergence criterion

The main solutions to these problems are:

- ❖ Verify that the problem is well-posed.
- ❖ Compute an initial solution using a first-order discretization scheme.
- ❖ Reduce the under-relaxation factors.
- ❖ Remeshing or refining the geometry cells.

I.18.4 Mesh Study

Discretization is essential in numerical computing. A quality mesh improves accuracy, but excessive refinement increases computational time. Therefore, it is necessary to balance accuracy and efficiency

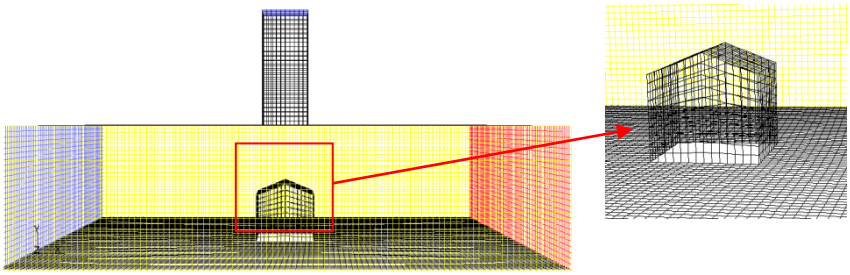

Figure III.16: Computational mesh

I.19 Conclusion

In this chapter presented the main numerical approaches used in fluid mechanics with focus on the finite volume method the concepts of meshing, as well as generation and simulation tools such as GAMBIT and FLUENT, were introduced the numerical solution steps were detailed to prepare for the analysis the results in the next chapter.

Chapter IV:

Results and Discussion

I.20 Introduction

In this final chapter, we will numerically investigate the forced convection airflow around a heated electronic component at 75°C. The obtained results use the SST (Shear Stress Transport) numerical model to examine thermal and dynamic profiles. These findings demonstrate the effect of component geometry, jet velocity, and injection parameters (crossfolow) on the thermal performance improvement of these electronic parts.

I.21 Results Analysis and Interpretation of Data

I.21.1 CFD Results Validation

In order to verify the accuracy of the present results, the validation of the turbulence model SST k-ω was performed for turbulent flow fields in a finned stator. Figure IV.1 shows the variation of the velocity compared with those published by the experimental study [33]. The Figure represents the variation of the y/h as a function of the velocity U/U_j for the regular cube of the electronic component. The comparison shows good agreement between our numerical results and the experimental data.

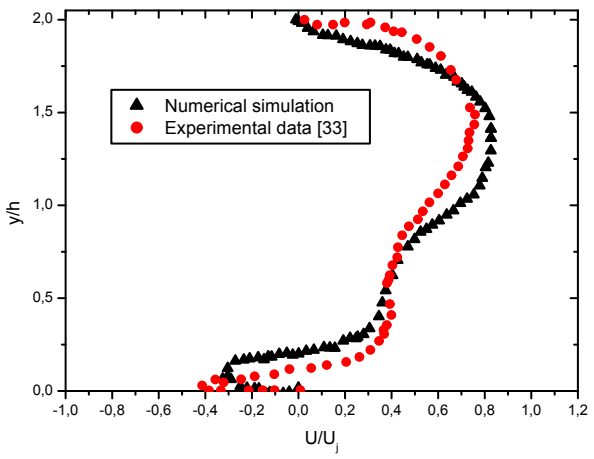

X/h=-0.75

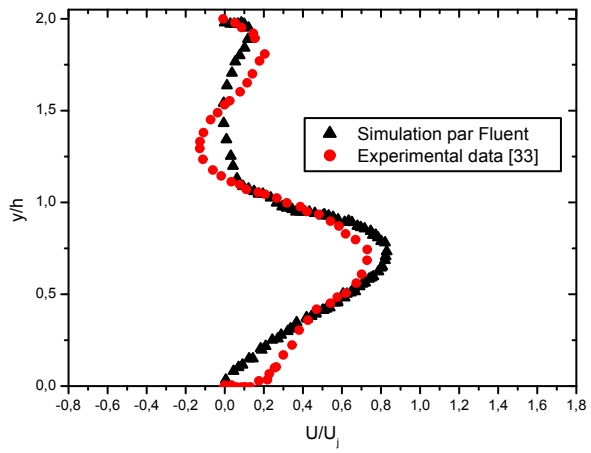

X/h=1.5

Figure IV.1: Comparison of present numerical results with the experimental results

I.21.2 Impact of V-shaped groove mounted internally and externally on the electronic component

I.21.2.1 Thermal effect

I.21.2.1.1 Contours of temperatures according to the plane XY with Z/h= 0

For Re_{in}=3410 and Re_{jet}=1705, this figure shows the temperature distribution at a horizontal cross-section (Z/h = 0). For the regular cube, high temperatures appear at the center of the component's surface, indicating heat accumulation. When a V-shaped groove is mounted inside the component with four different values of P (P=-0.05, -0.1, -0.15, -0.2), heat is more evenly distributed, allowing better internal cooling. With a V-shaped groove mounted outside the component with same values of P (P=0.05, 0.1 ,0.15, 0.2), the temperature significantly drops at the top region, showing improved surface cooling due to direct airflow. By efficiently controlling the thermal wake and stagnation zone downstream of the heated component, the V-shaped groove installed outside the component with depth ratio P=0.2 achieves optimal cooling, according to thermal contour analysis (Fig. IV.2). In order to prevent hot fluid recirculation, which would otherwise hinder heat transfer, the external configuration with P=0.2 produces improved flow mixing that dramatically decreases the thermal wake region. In order to improve fluid exchange and heat dissipation from the 75°C surface, the deeper groove creates powerful secondary flows that break up the stagnation zone. The external V-groove, as opposed to internal mounting, permits unhindered jet impingement while generating advantageous flow

disturbances that lessen the thickness of the thermal boundary layer and the effects of stagnation behind the component.

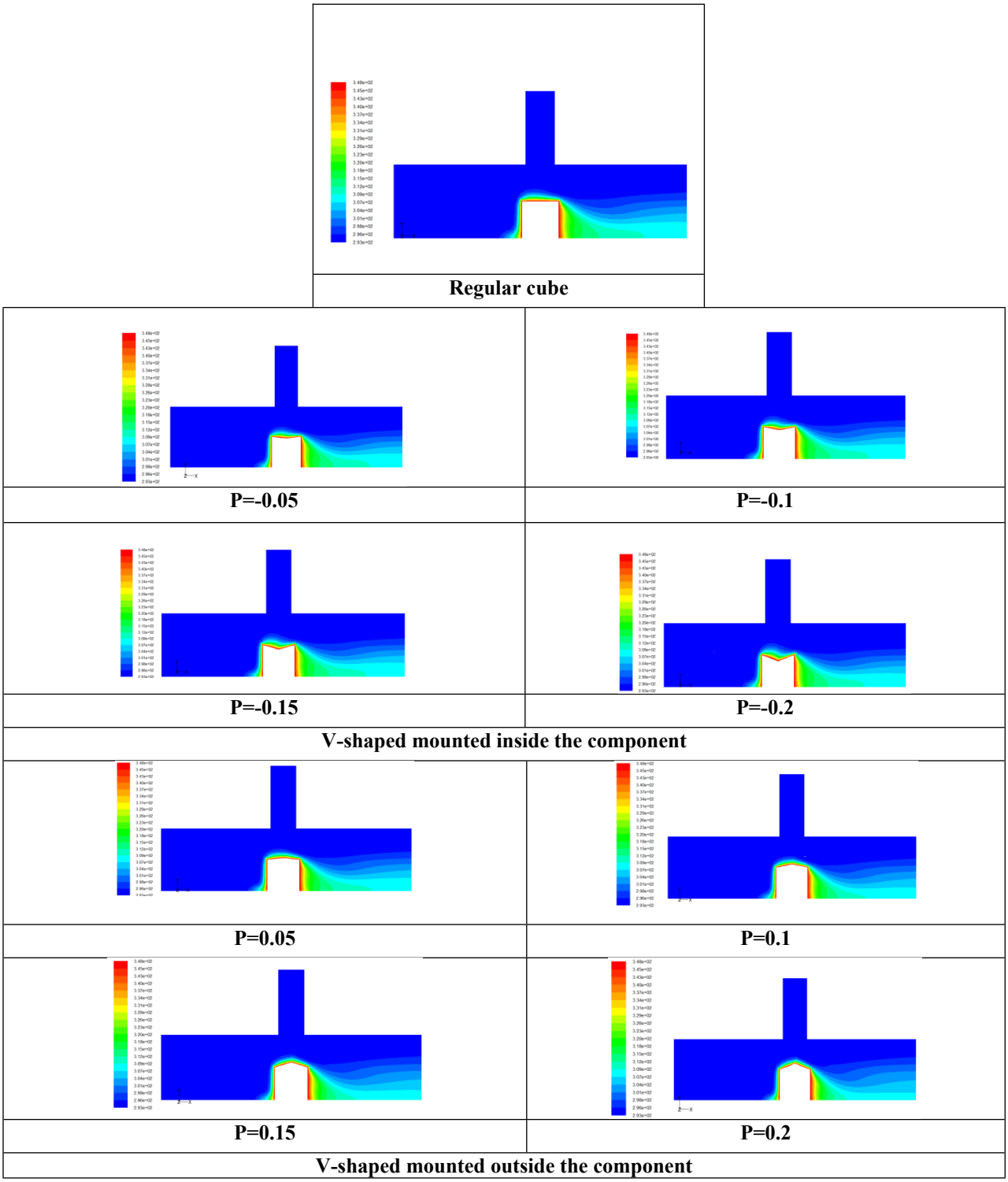

Figure IV.2: Temperature contours comparison according the plane XY à Z/h=0

I.21.2.1.2 Contours of temperatures according to the plane XZ with Y/h= 0.5(for y=0.5, the middle of the component)

The temperature distribution through the center of the heated electronic component across various V-groove configurations is shown by the thermal contours at the mid-plane (XZ at Y/H=0.5) in Figure IV.3. Heat stays concentrated in the center of the Regular cube. Heat moves toward the surface of the component thanks to a V-shaped groove installed inside. The component's exterior has a V-shaped groove that lets cold air pass over the top, lowering the temperature there. By minimizing the high-temperature zone downstream of the component and producing the most compact thermal wake, the external V-groove mounting with P=0.2 exhibits superior thermal performance. marked thermal improvements, with wider thermal wakes and bigger stagnation zones that prevent the 75°C component surface from transferring heat as efficiently as possible. As demonstrated by the narrower thermal plume and lower peak temperatures in comparison to the standard cube and other groove depths, this configuration successfully decreases the stagnation zone size and encourages improved heat dissipation. The external configuration's gradual improvement from P=0.05 to P=0.2 demonstrates improved convective cooling and more efficient thermal boundary layer disruption. Conversely, the internal V-groove configurations show less noticeable thermal improvements, with more extensive thermal wakes and larger stagnation zones that prevent the 75°C component surface from transferring heat as efficiently as possible.

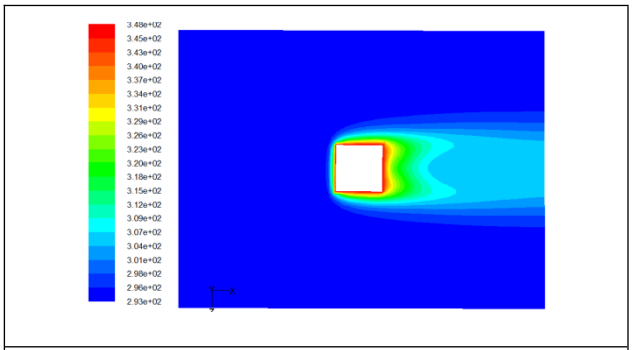

Regular cube

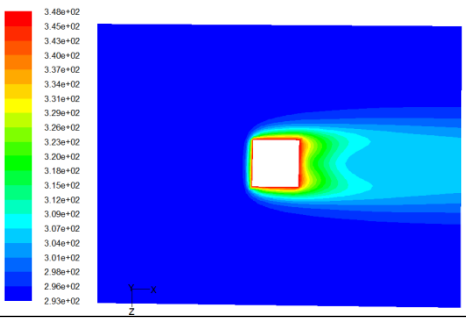

P=-0.05

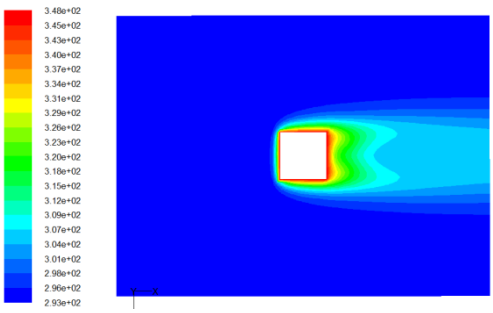

P=-0.1

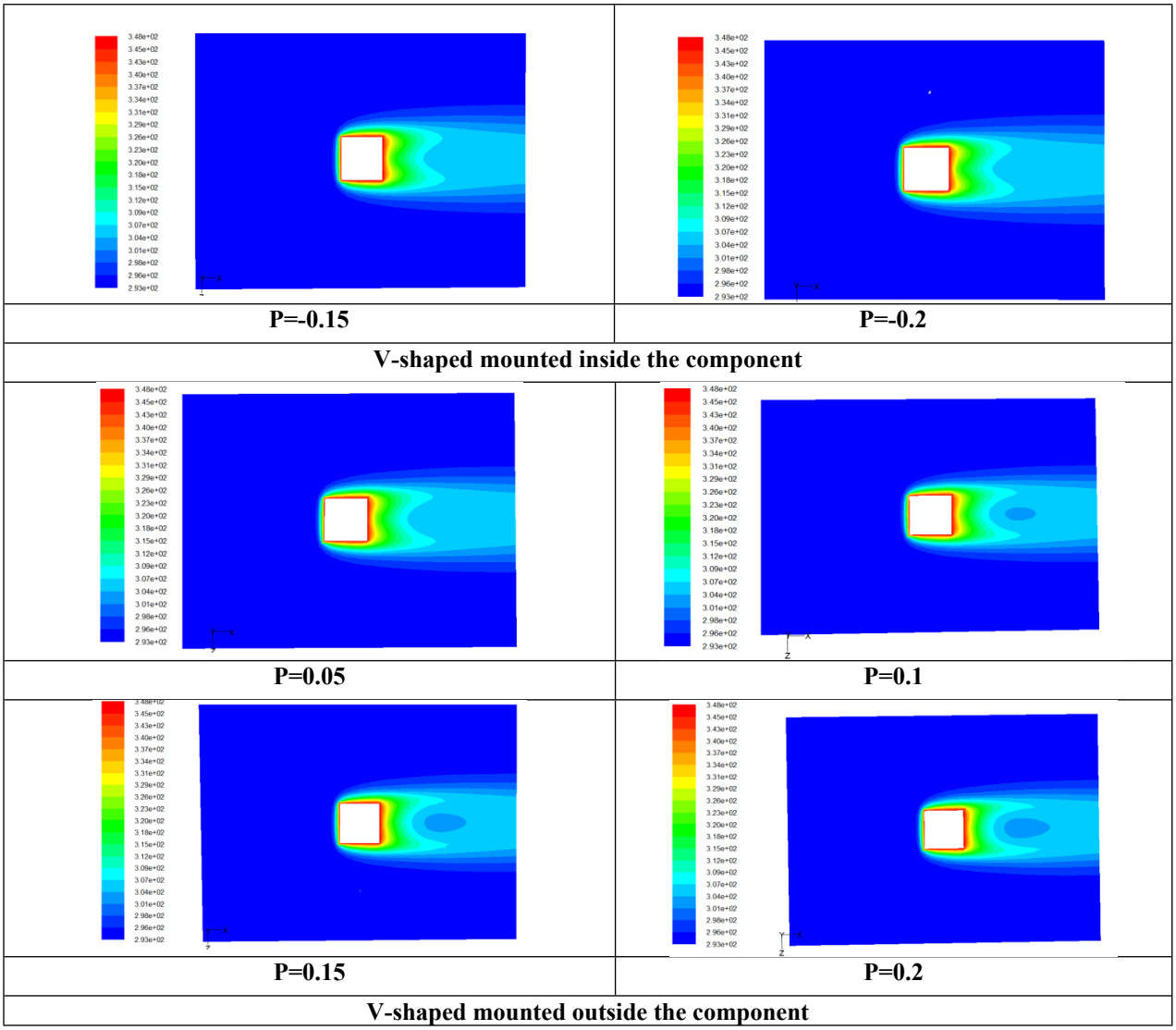

Figure IV.3. Temperature contours comparison according the plane XZ at Y/h=0.5 for Re_{in} =3410

I.21.2.1.3 Thermal profiles

The temperature evolution at X/H=-0.75 (upstream of the component) is depicted in Figure IV.4, where all configurations show comparable temperature profiles of 20–22°C, suggesting little upstream thermal influence. Minor preheating effects from the approaching flow interacting with the heated component geometry are suggested by the slight variations near the wall(Y/Happroaching0).

Significant thermal stratification is visible in Figure IV.5, which shows temperature profiles at X=0.5 (directly downstream of the component), with peak temperatures approaching 70°C close to the component surface. In comparison to the standard cube and internal configurations (down

0.1, down 0.2), the external V-groove configurations (up 0.1, up 0.2) exhibit better cooling performance with65 lower peak temperatures and steeper thermal gradients, suggesting improved heat dissipation and a thinner thermal boundary layer.

The temperature evolution at X=1 (further downstream), where thermal wakes are easily distinguished between configurations, is shown in Figure IV.6. While the regular cube maintains the highest thermal wake temperatures, the external V-groove with P=0.2 (up 0.2) exhibits the best thermal recovery with lower downstream temperatures and faster thermal mixing. Better thermal wake management and improved convective cooling across the downstream region are two examples of how external configurations routinely perform better than internal ones.

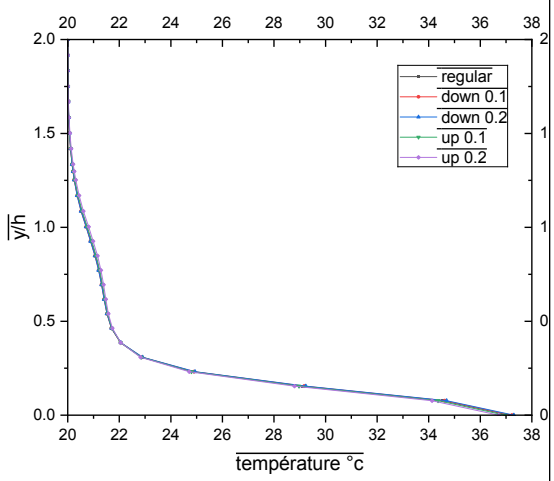

Figure IV.4: Temperature evolution for different configurations at X/h=-0.75

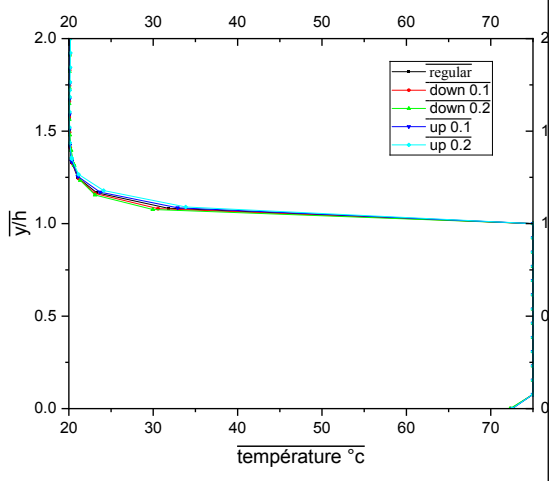

Figure IV.5: Temperature evolution for different configurations at X=0.5

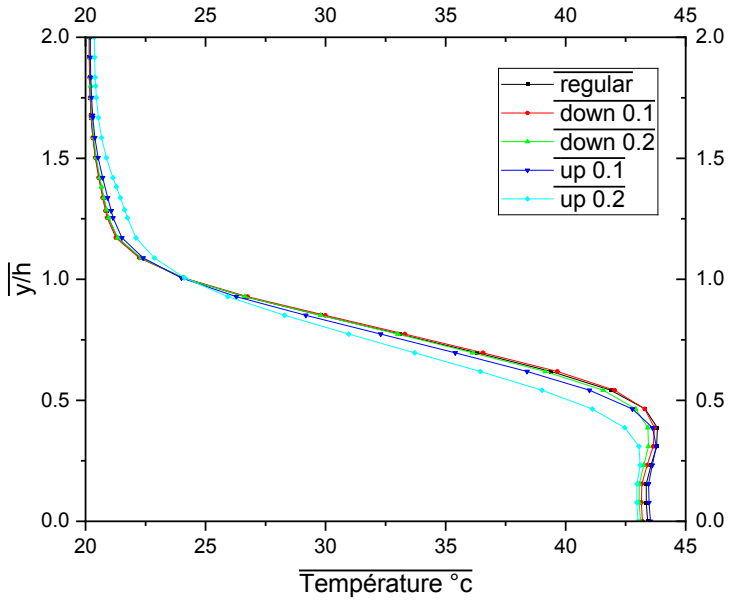

Figure IV.6: Temperature evolution for different configurations at X=1

I.21.2.1.4 Dynamic effect

I.21.2.1.4.1 Contours of velocity according to the plane XY with Z/h= 0

For Reynolds number 3410, Figure IV.7 compares various V-shaped groove configurations using velocity contours at the mid-plane (XY at Z/h=0). Downstream of the component, the regular cube baseline exhibits a typical wake formation and conventional flow separation with moderate velocity gradients. Although overall enhancement is limited by flow obstruction within the geometry, the internal V-groove configurations (P=0.05 to P=0.2) show progressive flow acceleration through the groove channels, with deeper grooves producing higher velocity jets that impinge on the component surface. Superior flow dynamics are demonstrated by the external V-groove configurations, especially at P=0.2, where the groove produces powerful secondary flows and improved velocity gradients that facilitate improved heat transfer and mixing. The external mounting creates advantageous flow disturbances that break stagnation zones and permits unhindered flow acceleration around the component. Significantly, the external configurations exhibit stronger flow recirculation patterns and more noticeable velocity variations, which enhance convective cooling. The P=0.2 case exhibits the best flow mixing and velocity distribution for the best thermal performance.

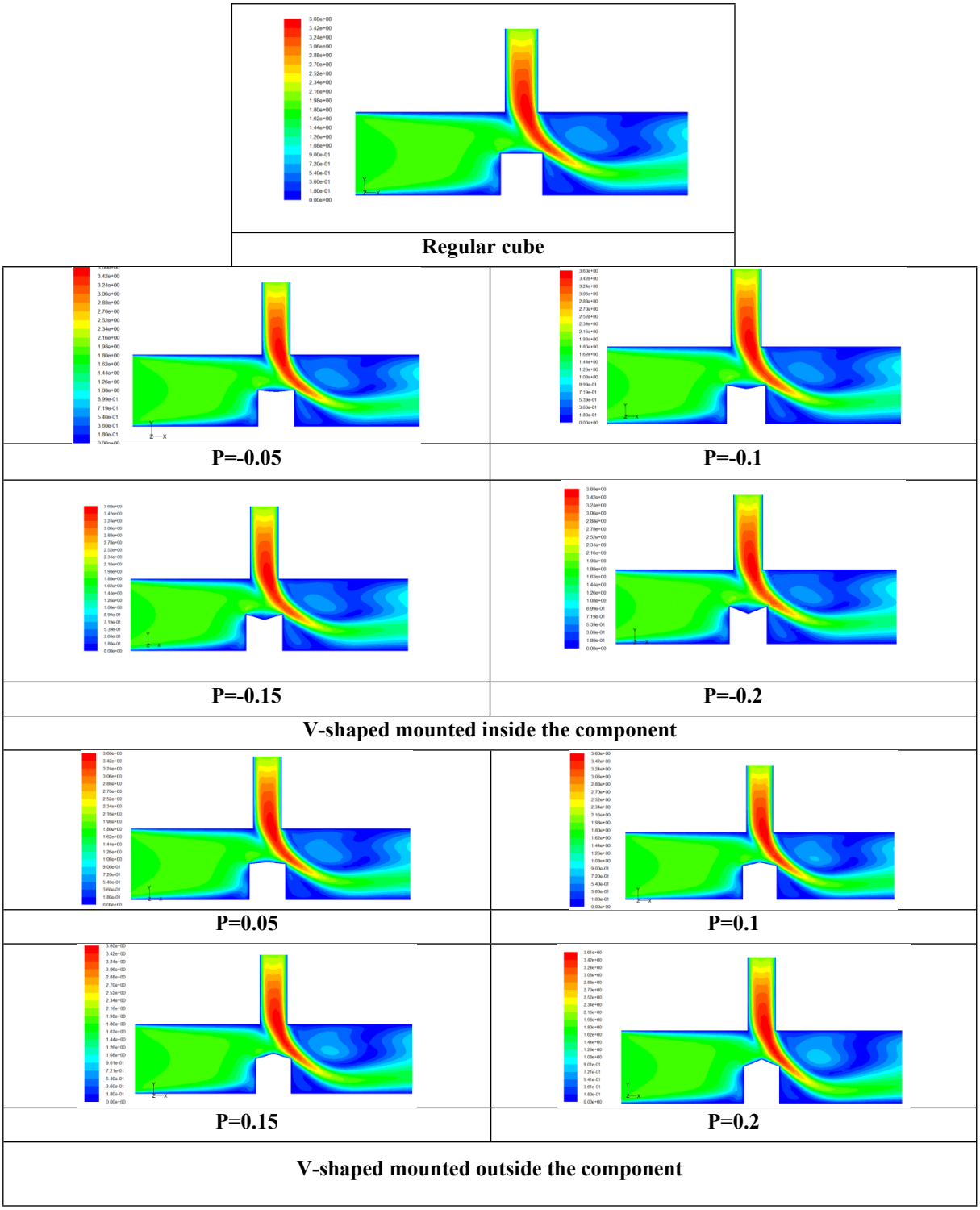

Figure IV.7: Comparison of velocity contours for different configurations of V-shaped groove along the plane XY at Z/h=0 pour Re_{in} =3410

I.21.2.1.4.2 Streamlines

Flow behavior around various V-shaped groove configurations is depicted by streamline patterns at the mid-plane (XY at Z/h=0) in Figure IV.8. Downstream of the component, the regular cube displays typical flow separation with sizable recirculation zones and comparatively straightforward streamline patterns. Although internal mounting restricts overall flow enhancement, streamlines indicate stronger flow acceleration through the groove channels and improved flow reattachment downstream in the internal V-groove configurations, which show gradually enhanced flow mixing as groove depth increases from P=0.05 to P=0.2. Better turbulent mixing and flow disturbances are indicated by the external V-groove configurations' more intricate streamline patterns and superior flow dynamics. The most noticeable flow manipulation is seen in the external P=0.2 configuration, where streamlines reveal strong secondary flows, improved wake mixing, and increased flow separation and reattachment cycles, all of which improve heat transfer. With deeper grooves producing stronger vortical structures that encourage thermal boundary layer disruption and improved cooling performance, the streamline visualization demonstrates how external mounting produces more effective flow disruption and enhanced convective transport when compared to internal configurations.

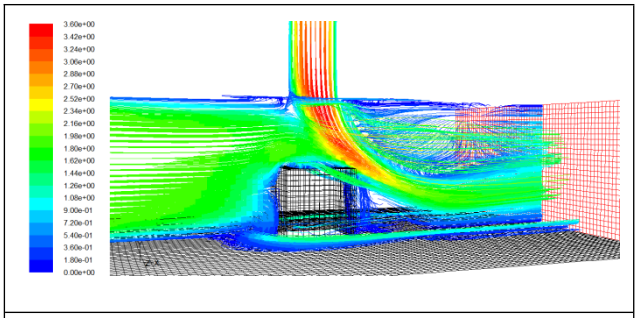

Regular cube

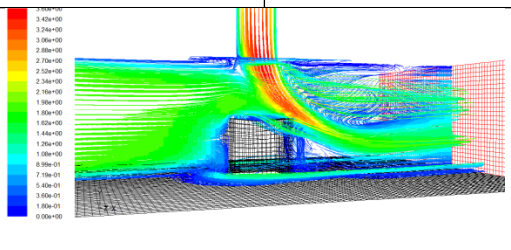

P=-0.05

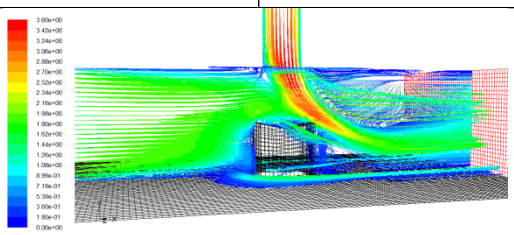

P=-0.1

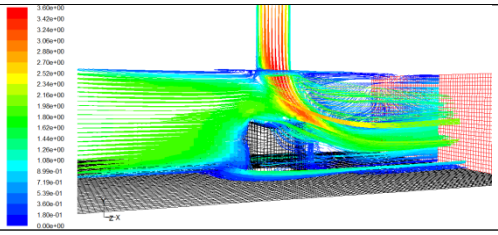

P=-0.15

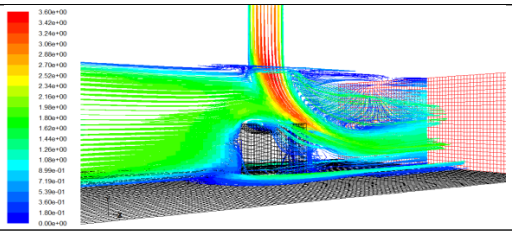

P=-0.2

V-shaped mounted inside the component

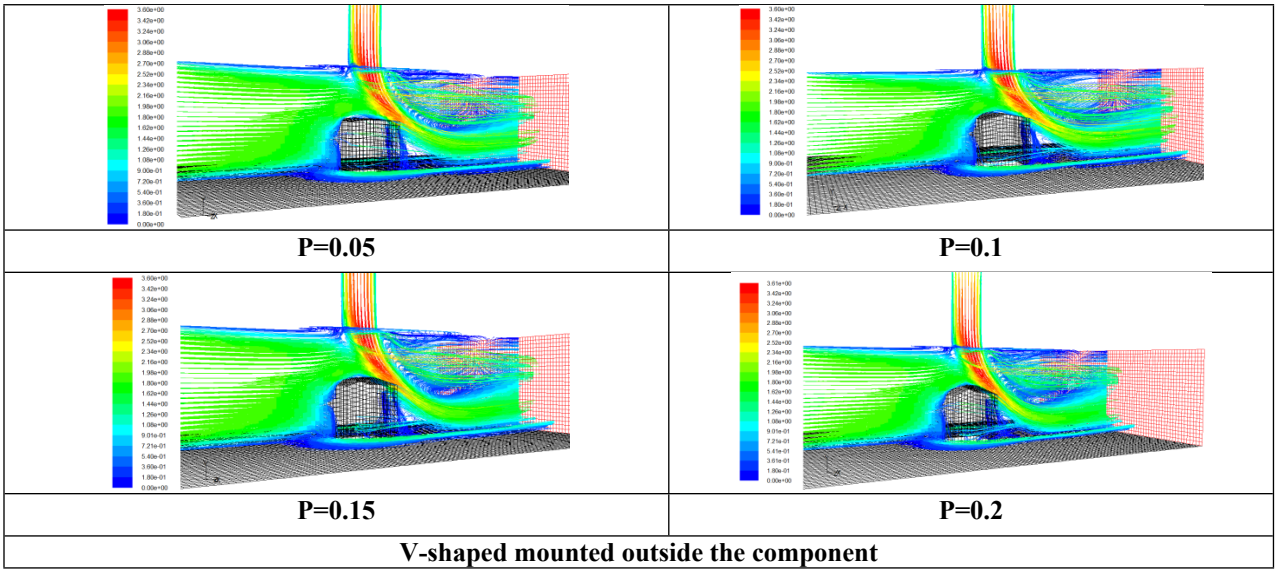

Figure IV.8: Comparison of streamlines for different configurations of V-shaped groove along the plane XY at Z/h=0

For various V-shaped groove configurations, Figure IV.9 shows streamline patterns at the mid-plane (XZ at y/h=0.5), exposing flow behavior through the heated electronic component's center. With a sizable stagnation zone and a straightforward downstream recirculation pattern, the regular cube exhibits conventional flow separation, resulting in limited flow mixing and enhanced heat transfer. Although the internal mounting limits overall flow development and mixing effectiveness as groove depth increases from P=0.05 to P=0.2, the internal V-groove configurations demonstrate a moderate improvement in flow, with streamlines indicating enhanced flow acceleration through the groove channels. The flow dynamics of the external V-groove configurations are noticeably better, with more intricate streamline patterns that show increased turbulent mixing and flow disturbances surrounding the component. The most noticeable flow manipulation is seen in the external P=0.2 configuration, where streamlines show multiple recirculation zones, strong secondary flows, and enhanced wake mixing that successfully disrupt the thermal boundary layer. In comparison to both the standard cube and internal groove configurations, the streamline visualization clearly shows how external mounting produces stronger vortical structures that promote enhanced convective heat transfer and reduced thermal wake formation by facilitating more efficient flow separation and reattachment cycles.

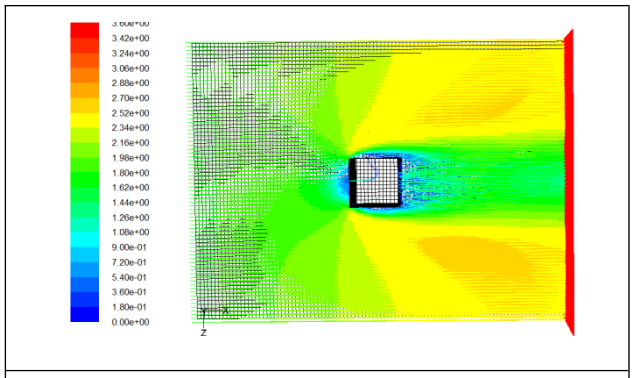

Regular cube

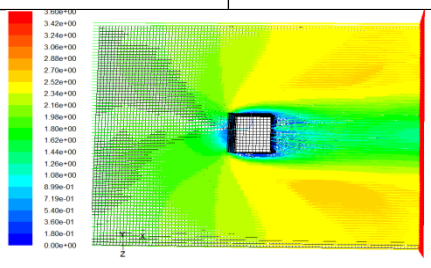

P=-0.05

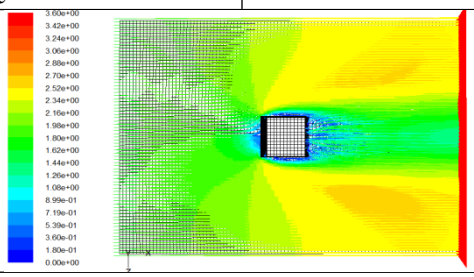

P=-0.1

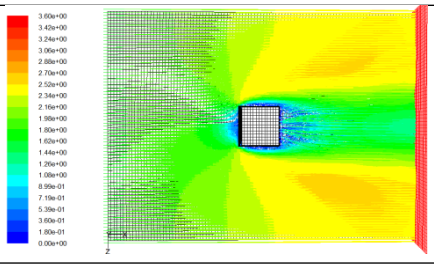

P=-0.15

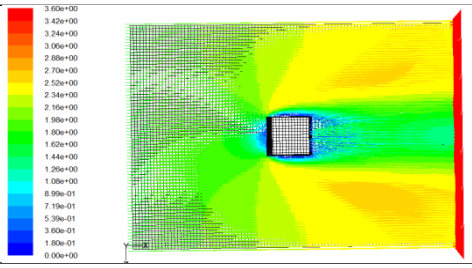

P=-0.2

V-shaped mounted inside the component

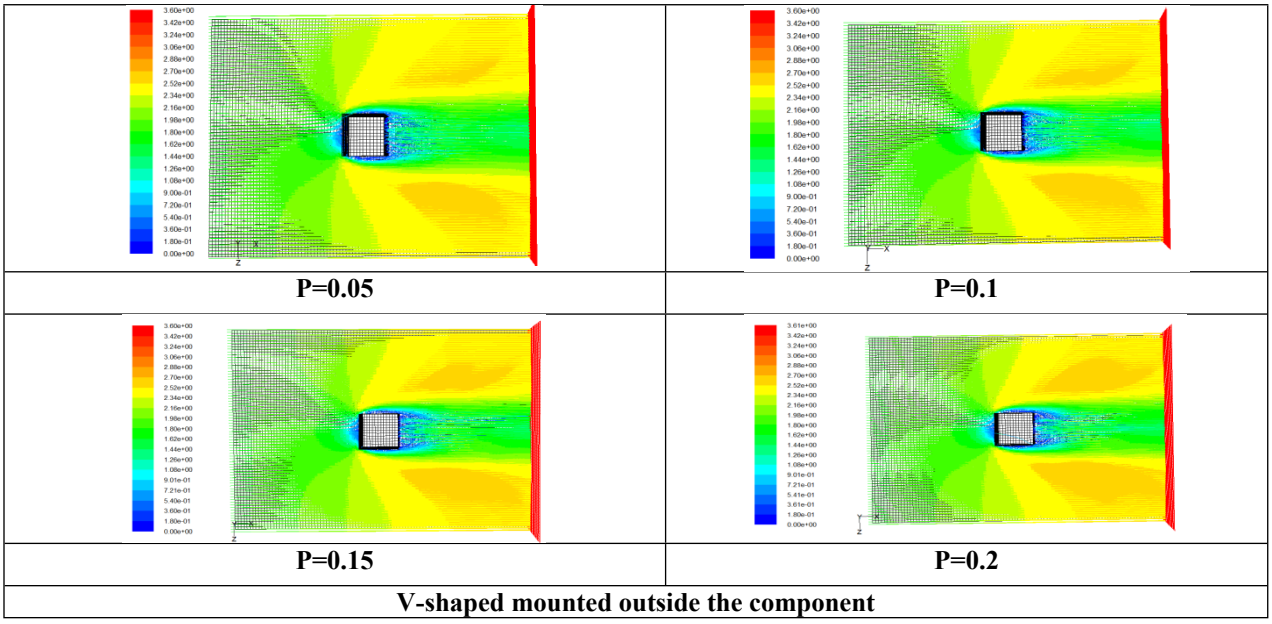

Figure IV.9: Comparison of streamlines for different configurations of V-shaped groove along the plane XZ at y/h=0.5

I.21.2.1.5 Velocity profiles

At X=-0.75 (upstream of the component), where all configurations display nearly identical velocity profiles, Figure IV.10 illustrates velocity evolution, suggesting little influence from upstream flow. All configurations exhibit the same boundary layer development pattern, and the smooth velocity distribution shows fully developed flow conditions prior to encountering the component.

The figure IV.11 shows velocity profiles at X=0.5, which is directly downstream of the component. The various groove configurations cause notable flow changes. In comparison to the standard cube and internal configurations (down 0.1, down 0.2), the external V-groove configurations (up 0.1, up 0.2) exhibit greater velocity acceleration and more noticeable velocity gradients. The external P=0.2 case exhibits the strongest flow acceleration and the highest velocity peaks, suggesting better flow mixing and improved momentum transport, both of which improve heat transfer performance.

The velocity evolution at X=1 (further downstream), where different wake characteristics are visible between configurations, is shown in Figure IV.12. The regular cube maintains the most noticeable velocity deficit in the wake region, whereas the external V-groove with P=0.2 (up 0.2) shows the best wake recovery with higher velocity levels and better flow reattachment.

When compared to internal configurations, the external ones consistently show better flow recovery and less wake formation, suggesting improved flow mixing and momentum transport, which is directly related to better thermal performance.

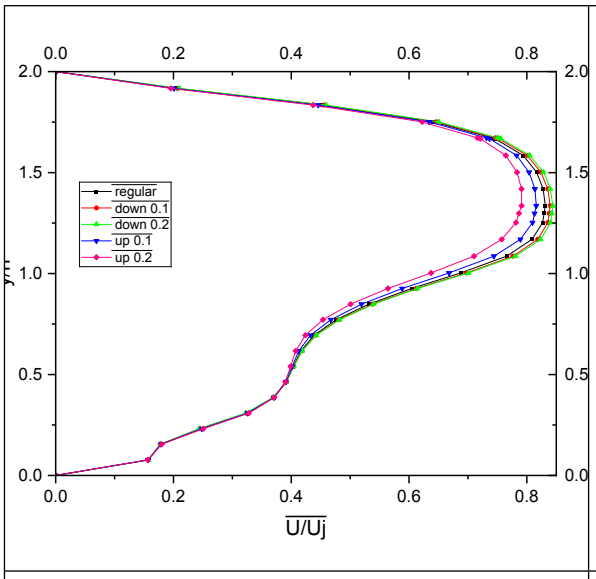

Figure IV.10: Velocity evolution for different configurations at X=-0.75

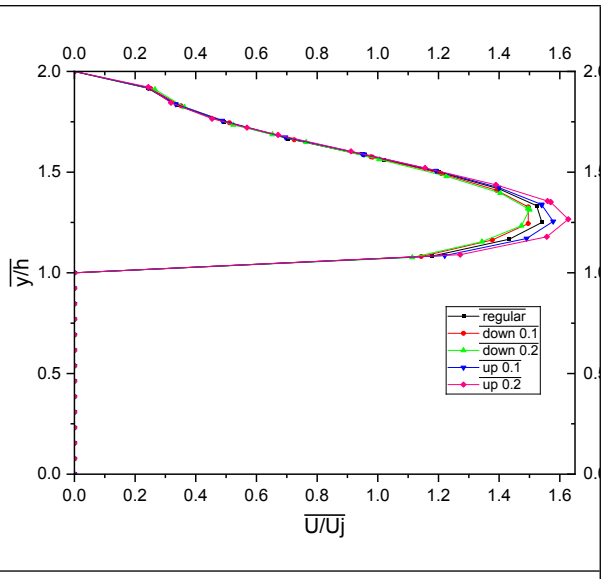

Figure IV.11: Velocity evolution for different configurations at X=0.5

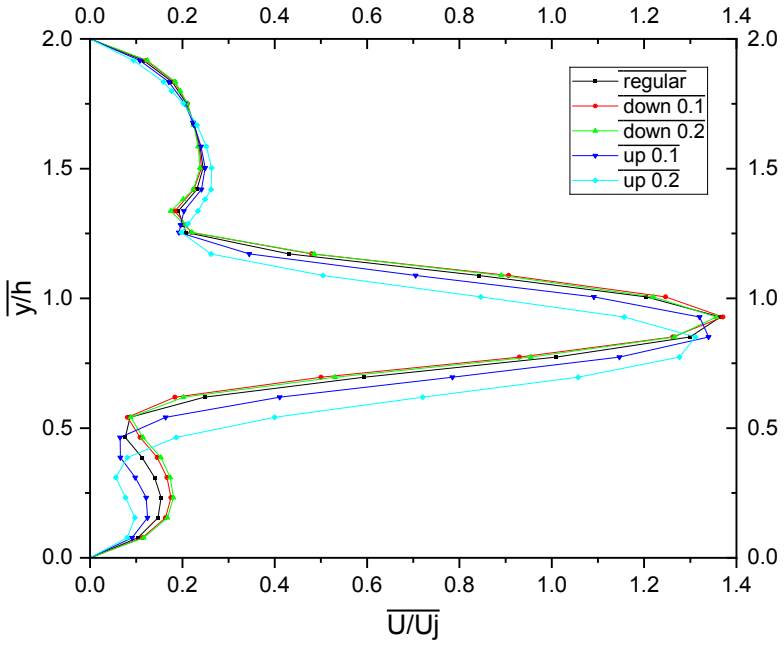

Figure IV.12: Velocity evolution for different configurations at X=1

I.21.3 Impact of Reynolds numbers

I.21.3.1 Variation of air jet Reynolds numbers

I.21.3.1.1 Contours of temperatures according to the plane XY with Z/h= 0

The figure IV.13 shows temperature contours at the mid-plane (XY at Z/h=0) for three different configurations with constant crossflow Reynolds number (Rein = 3410) and varying air jet Reynolds numbers (Rej = 1705, 3410, and 5115). With a regular cube baseline and traditional thermal wake patterns that gradually get better as the jet Reynolds number rises, configuration (a) exhibits less thermal buildup and smaller stagnation zones at higher jet velocities. The internal V-shaped groove (P=0.2) in configuration (b) shows moderate thermal improvements over the standard cube. At higher Reynolds numbers, the enhanced cooling becomes more noticeable because of increased jet impingement through the groove channels. With the most compact thermal wakes and efficient heat dissipation, the external V-shaped groove (P=0.2) in configuration (c) exhibits superior thermal performance across all Reynolds numbers. At higher jet Reynolds numbers, the external configuration exhibits the greatest thermal enhancement, resulting in ideal flow mixing and heat transfer augmentation. All configurations experience

improved cooling as the jet Reynolds number rises from 1705 to 5115, but the external V-groove continuously maintains the lowest component temperatures and the best thermal wake management, demonstrating its superior thermal performance under a range of flow conditions.

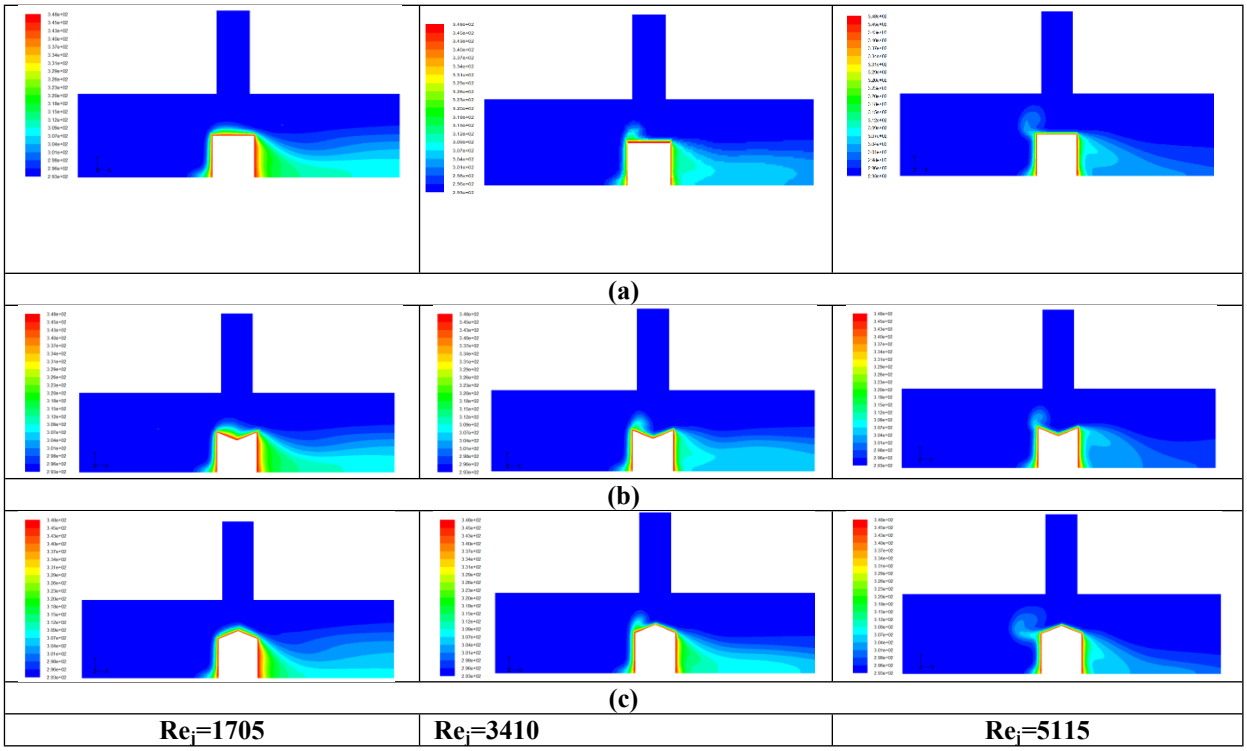

Figure IV.13: Temperature contours for different air jet Reynolds at Re_{in} =3410: a-Regular cube,b-V-shaped mounted inside the cube with (P=-0.2),c-V-shaped mounted outside the cube with (P=0.2)

I.21.3.1.2 Thermal profile

Temperature evolution at X/H=1 (downstream of the component) for three configurations with different air jet Reynolds numbers (Rej=1705, 3410, and 5115) while keeping the crossflow Reynolds number constant (Rein = 3410) is shown in Figure IV.14. All configurations exhibit notable thermal wake effects at the lowest jet Reynolds number (Rej=1705), with the external V-groove (up 0.2) showing the best thermal recovery and the regular cube showing the highest downstream temperatures. All configurations show improved cooling as the jet Reynolds number rises to 3410, with the external V-groove continuing to perform better due to lower peak temperatures and steeper thermal gradients that indicate better heat dissipation. The cooling enhancement is most noticeable at the highest jet Reynolds number (Rej=5115), where the external V-groove configuration achieves the lowest downstream temperatures and the best thermal wake management. Though it consistently performs worse than the external

configuration, the internal V-groove (down 0.2) exhibits a moderate improvement over the regular cube across all Reynolds numbers. Through superior flow mixing and heat transfer augmentation in the component wake region, the external V-groove continuously provides optimal thermal performance, as evidenced by the progressive temperature reduction with increasing jet Reynolds number.

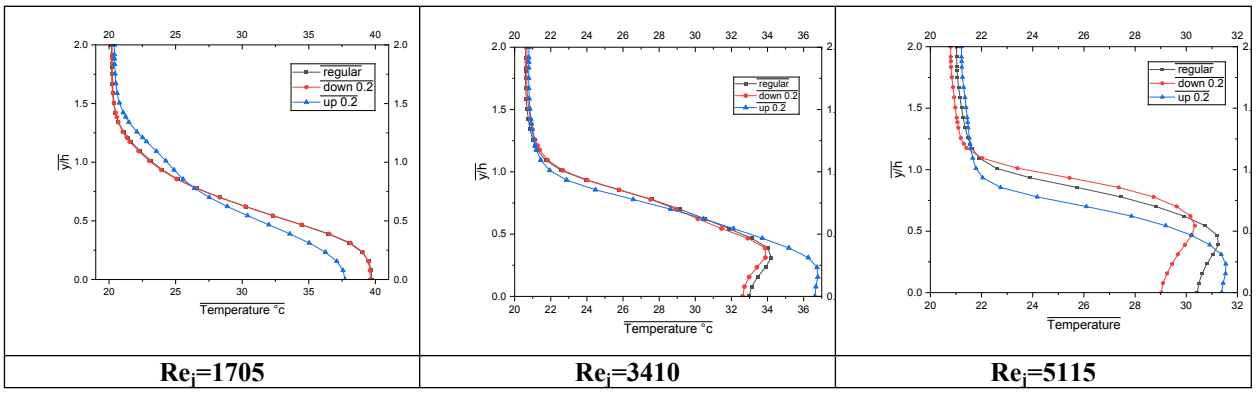

Re_j=1705	Re_j=3410	Re_j=5115

Figure IV.14: Temperature evolution for different air jet Reynolds at Re_{in} =3410: a-Regular cube, b-V-shaped mounted inside the cube with (P=-0.2), c-V-shaped mounted outside the cube with (P=0.2)

I.21.3.1.3 streamlines

According to the plane XY

For three configurations with different air jet Reynolds numbers (Rej=1705, 3410, and 5115) and a constant crossflow Reynolds number (Rein=3410), Figure IV.15 shows streamline patterns at the mid-plane (XY at Z/h=0). As the jet Reynolds number rises, the regular cube with traditional flow separation patterns in configuration (a) becomes more ordered and displays stronger recirculation zones, suggesting improved flow mixing downstream. In contrast to the standard cube, configuration (b) shows the internal V-shaped groove (P=0.2) with gradually improved flow acceleration through the groove channels as the jet Reynolds number increases. This results in more noticeable flow disturbances and improved mixing. In contrast to the standard cube, configuration (b) shows the internal V-shaped groove (P=0.2) with gradually improved flow acceleration through the groove channels as the jet Reynolds number increases. This results in more noticeable flow disturbances and improved mixing. With stronger secondary flows and improved vertical structures that facilitate superior heat transfer, configuration (c) shows the external V-shaped groove (P=0.2) with the most intricate and efficient streamline patterns across all Reynolds numbers. All configurations exhibit increased flow complexity and mixing as the jet Reynolds number rises from 1705 to 5115, but the external V-groove consistently produces the most noticeable flow disturbances and the best streamline patterns. Stronger turbulent mixing is produced by the external configuration's

superior flow manipulation, which includes more efficient flow separation and reattachment cycles. This leads to better thermal performance throughout the Reynolds number range.

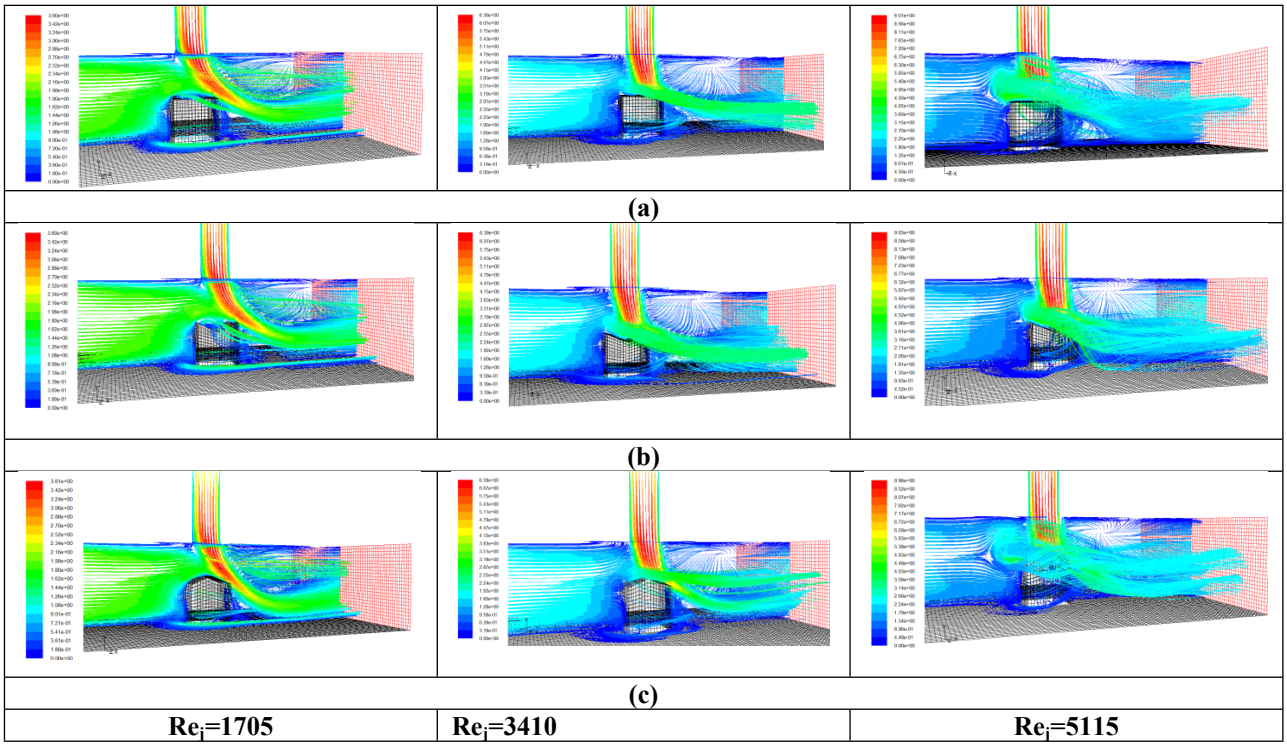

Figure IV.15: Comparison of streamlines for different jet Reynolds numbers along the plane XY at Z/h=0

According the plane XZ with Y/h= 0.5(for y=0.5, the middle of the component)

For three configurations with different air jet Reynolds numbers (Rej=1705, 3410, and 5115) and a constant crossflow Reynolds number (Rein=3410), Figure IV.16 shows streamline patterns at the mid-plane (XZ at y/h=0.5). The regular cube with traditional flow separation and wake formation is depicted in configuration (a), which shows improved downstream mixing and fewer stagnation zones as the jet Reynolds number increases. The internal V-shaped groove (P=0.2) in configuration (b) shows a moderate flow enhancement with streamlines that show better wake recovery and flow acceleration through the groove channels as the jet Reynolds number rises from 1705 to 5115. The internal V-shaped groove (P=0.2) in configuration (b) shows a moderate flow enhancement with streamlines that show better wake recovery and flow acceleration through the groove channels as the jet Reynolds number rises from 1705 to 5115. The external V-shaped groove (P=0.2) in configuration (c) exhibits the most intricate and efficient streamline patterns at all Reynolds numbers. Its enhanced vertical structures and noticeable secondary flows produce superior flow mixing around the component. Multiple recirculation zones that successfully disrupt the thermal boundary layer are produced by the external configuration, which exhibits the most significant flow manipulation with stronger flow

separation and reattachment cycles. In comparison to both the standard cube and internal groove configurations, the external V-groove continuously maintains the best wake management and the most efficient flow disturbances as the jet Reynolds number rises, resulting in improved turbulent mixing and better thermal performance.

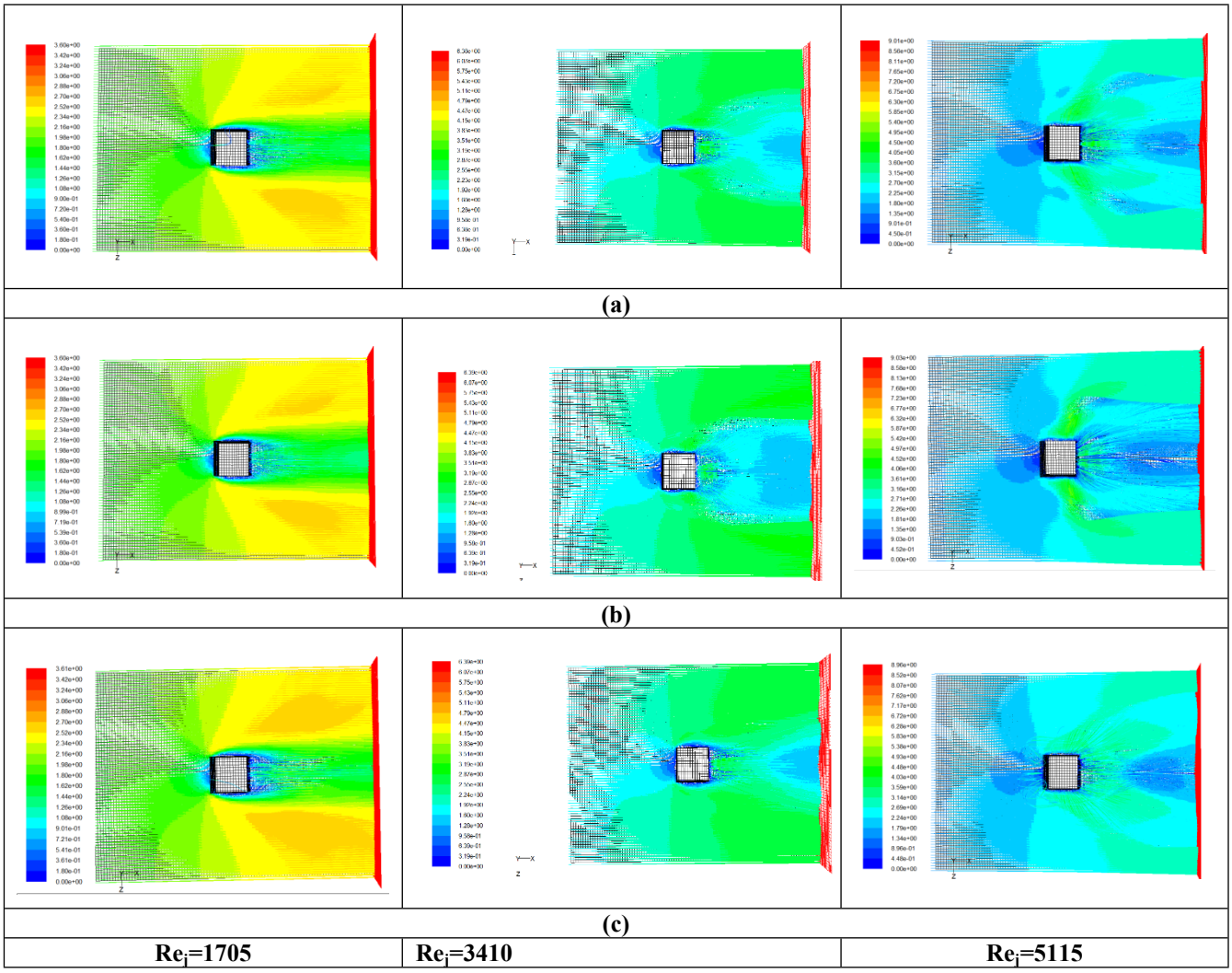

Figure IV.16: Streamlines for different air jet Reynolds at Re_{in} =3410: a-Regular cube,b-V-shaped mounted inside the cube with (P=-0.2),c-V-shaped mounted outside the cube with (P=0.2)

IV.2.3.1.5. Velocity profiles :

At X/H=1 (downstream of the component), Figure IV.17 shows the evolution of velocity for three configurations with different air jet Reynolds numbers (Rej=1705, 3410, and 5115) while keeping the crossflow Reynolds number constant (Rein = 3410). All configurations display distinct velocity deficit regions typical of wake formation at the lowest jet Reynolds number

(Rej=1705), with the external V-groove (up 0.2) showing better wake recovery and the regular cube showing the most noticeable velocity reduction. All configurations show improved velocity recovery as the jet Reynolds number rises to 3410, with the external V-groove continuing to perform better thanks to higher velocity levels and smaller wake deficits, which suggest better momentum transport. The velocity enhancement is greatest at the highest jet Reynolds number (Rej=5115), where the external V-groove configuration achieves the highest downstream velocities and the most efficient wake recovery. In comparison to the baseline case, the internal V-groove (down 0.2) exhibits better velocity recovery and moderate improvement over the regular cube across all Reynolds numbers. The efficiency of improved jet impingement is demonstrated by the progressive velocity enhancement as the jet Reynolds number rises. The external V-groove continuously offers the best flow recovery through better momentum mixing and less wake formation downstream.

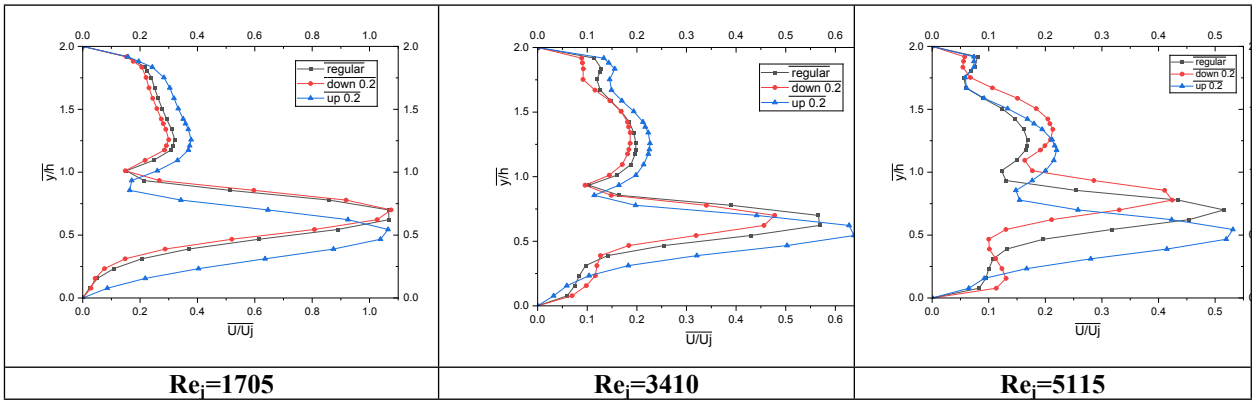

Re_j=1705	Re_j=3410	Re_j=5115

Figure IV.17: Velocity evolution for different air jet Reynolds at Re_{in}=3410: a-Regular cube, b-V-shaped mounted inside the cube with (P=-0.2), c-V-shaped mounted outside the cube with (P=0.2)

I.21.3.2 Variation of inlet Reynolds numbers

I.21.3.2.1 Contours of temperatures according to the plane XY with Z/h= 0

While keeping the jet Reynolds number constant (Rej=1705), Figure IV.18 shows temperature contours at the mid-plane (XY at Z/h=0) for three configurations across a range of inlet crossflow Reynolds numbers (Rein = 3410, 5752, and 8880). Configuration (a) displays a regular cube with typical thermal wake patterns that gradually get better as the crossflow Reynolds number rises. As the inlet velocity increases, there is less thermal buildup and more heat dissipation. When compared to the standard cube, configuration (b) shows the internal V-shaped groove (P=0.2) with moderate thermal improvements. The enhanced cooling becomes more noticeable at higher crossflow Reynolds numbers because of increased convective heat transfer through the groove channels. With the most compact thermal wakes and efficient heat

dissipation from the 75°C component, configuration (c) exhibits the external V-shaped groove (P=0.2) with superior thermal performance across all crossflow Reynolds numbers. At higher crossflow Reynolds numbers, the external configuration exhibits the greatest thermal enhancement, resulting in ideal flow mixing and convective cooling. The external V-groove continuously maintains the lowest component temperatures and the most efficient thermal wake management, confirming its superior performance under varying crossflow conditions while the jet impingement stays constant. All configurations benefit from enhanced cooling as the inlet Reynolds number increases from 3410 to 8880 due to increased convective heat transfer.

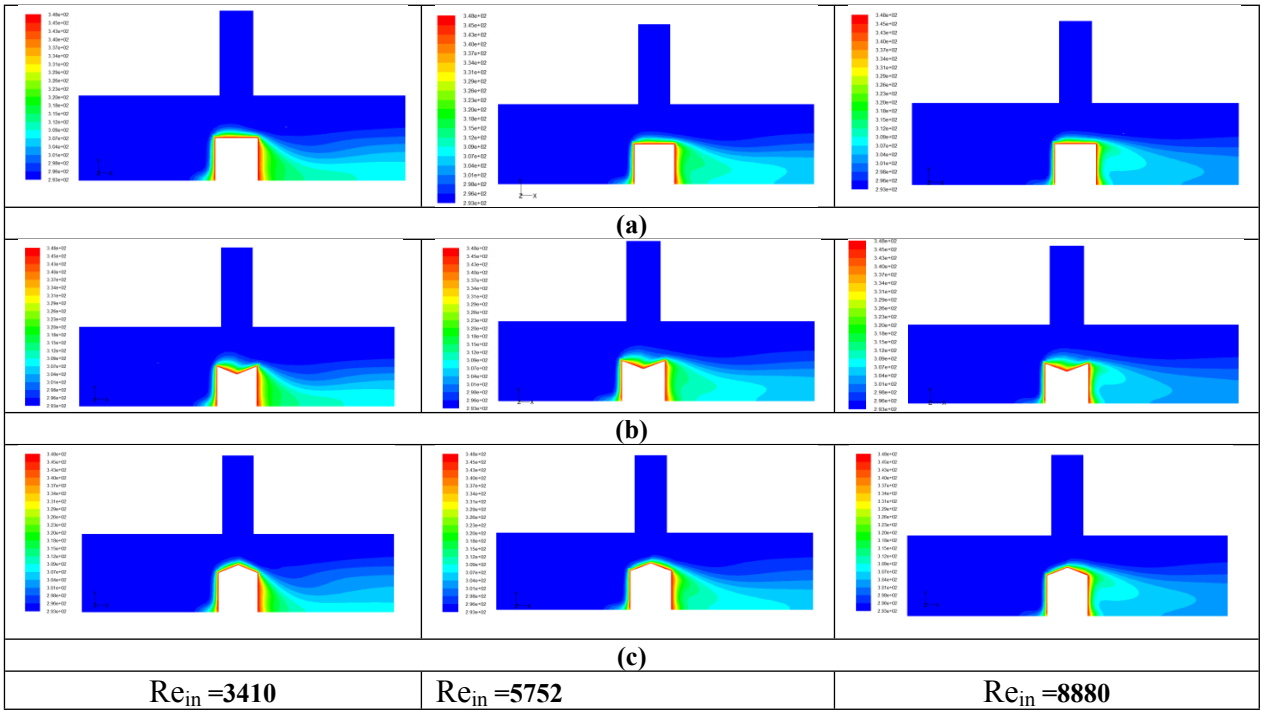

Figure IV.18: Temperature contours for different inlet Reynolds number at Re_j=1705:a-Regular cube,b-V-shaped mounted inside the cube with (P=-0.2),c-V-shaped mounted outside the cube with (P=0.2)

I.21.3.2.2 Thermal profiles

Temperature evolution profiles for three configurations with constant jet Reynolds number (Rej=1705) and varying inlet crossflow Reynolds numbers (Rein = 3410, 8880) are shown in Figure IV.19. With the lowest peak temperatures and steepest temperature gradients across all Reynolds numbers, the external V-shaped groove (P=0.2) exhibits superior thermal performance. It reaches roughly 33°C at Rein =3410 and 29°C at Rein =8880, as opposed to the

regular cube's 38°C and 34°C, respectively. The external V-groove's ideal flow mixing and convective heat transfer capabilities for cooling the 75°C electronic component are confirmed by the internal V-groove's moderate improvement over the standard cube and the increased crossflow Reynolds number, which improves cooling effectiveness for all configurations.

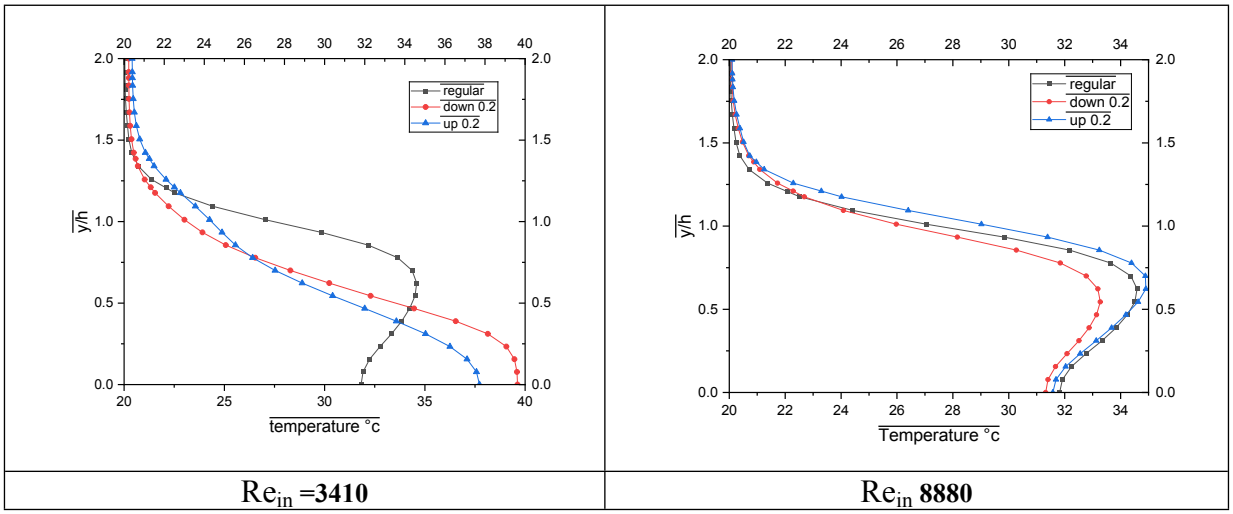

Re_{in} =3410	Re_{in} 8880

Figure IV.19: Temperature evolution for different inlet Reynolds number at Re_j=1705: a-Regular cube,b-V-shaped mounted inside the cube with (P=-0.2),c-V-shaped mounted outside the cube

I.21.3.2.3 streamlines

According the plane XY

Three configurations' streamlines are compared along the XY plane at Z/h=0 for different inlet Reynolds numbers (Rein = 3410, 5752, and 8880) in Figure IV.20. This shows how the flow field characteristics change as the crossflow velocity increases. While the regular cube (a) displays typical flow separation and wake formation behind the heated component, all configurations show comparatively weak and less structured flow patterns with limited circulation zones at the lowest Reynolds number (Rein = 3410). Stronger recirculation zones and improved mixing characterize the flow as the Reynolds number rises to 5752. This is especially noticeable in V-groove configurations, where the groove geometry starts to actively affect flow behavior. The external V-groove configuration (c) shows the most organized and dynamic flow field with optimal flow penetration around the component and improved mixing downstream, but all configurations show distinct and intense streamline patterns with well-defined circulation zones at the highest Reynolds number (Rein =8880). Improved convective heat transfer mechanisms are confirmed by the progressive strengthening of flow structures with increasing Reynolds number. The external V-groove continuously maintains superior flow organization and mixing characteristics, which are directly related to its improved thermal performance for cooling the electronic component.

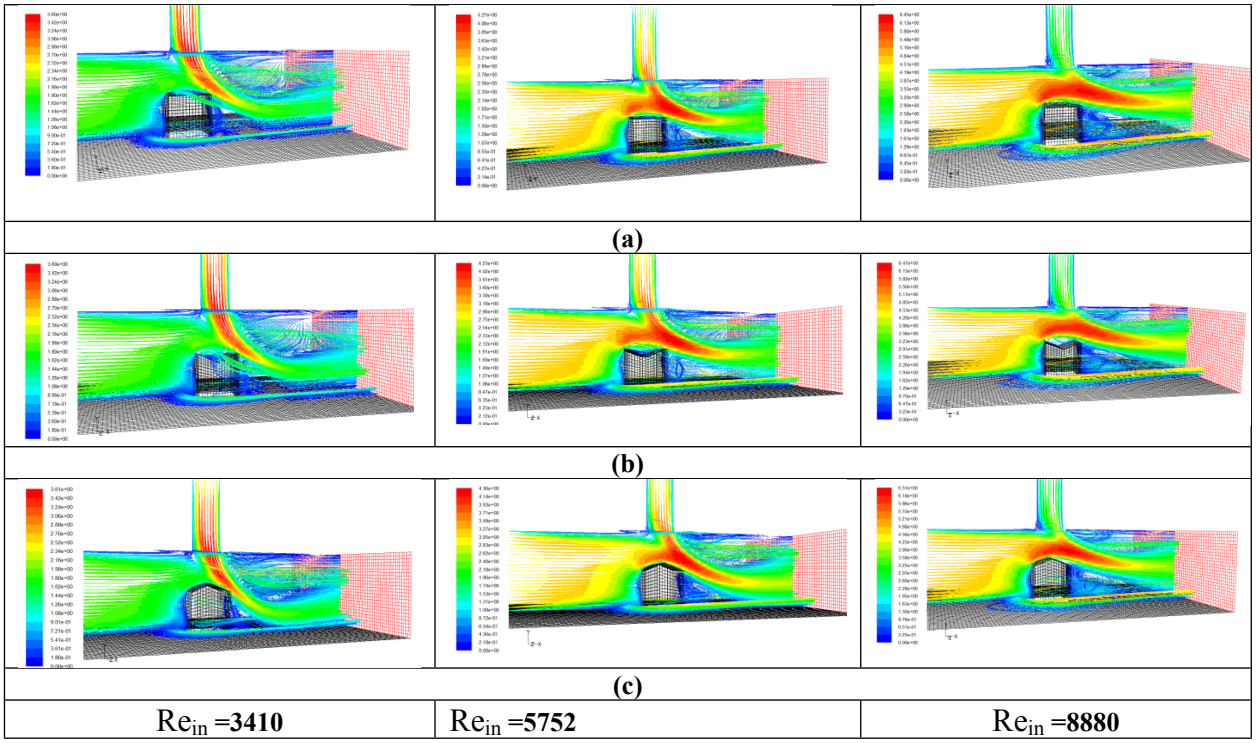

Figure IV.20: Comparison of streamlines for different inlet Reynolds numbers along the plane XY at Z/h=0

According the plane XZ with Y/h= 0.5(for y=0.5, the middle of the component)

The flow behavior at the mid-section of the component is shown by the streamlines for various inlet Reynolds numbers (Rein = 3410, 5752, 8880) along the XZ plane at Y/h=0.5, while maintaining a constant jet Reynolds number (Rej=1705). All configurations exhibit comparatively weak crossflow penetration at the lowest Reynolds number (Rein = 3410), with both V-groove configurations (b,c) displaying initial flow modification effects and the regular cube (a) displaying conventional flow patterns surrounding the heated component. When the Reynolds number rises to 5752, the flow intensifies and the crossflow-jet interaction becomes stronger. The external V-groove (c) shows better flow deflection and mixing characteristics around the component, while the internal V-groove (b) shows improved flow mixing within the groove cavity. All configurations benefit from strong crossflow effects at the highest Reynolds number (Rein =8880), but the external V-groove configuration (c) keeps the most ordered and active flow field with the best crossflow-jet interaction, which improves convective heat transfer from the component surfaces. As the Reynolds number increases, the flow patterns gradually change from weak to intense, illustrating the basic connection between crossflow velocity and cooling efficiency. The external V-groove continuously offers better flow organization and mixing, which is directly related to its improved thermal performance for the electronic component cooling application at 75°C.

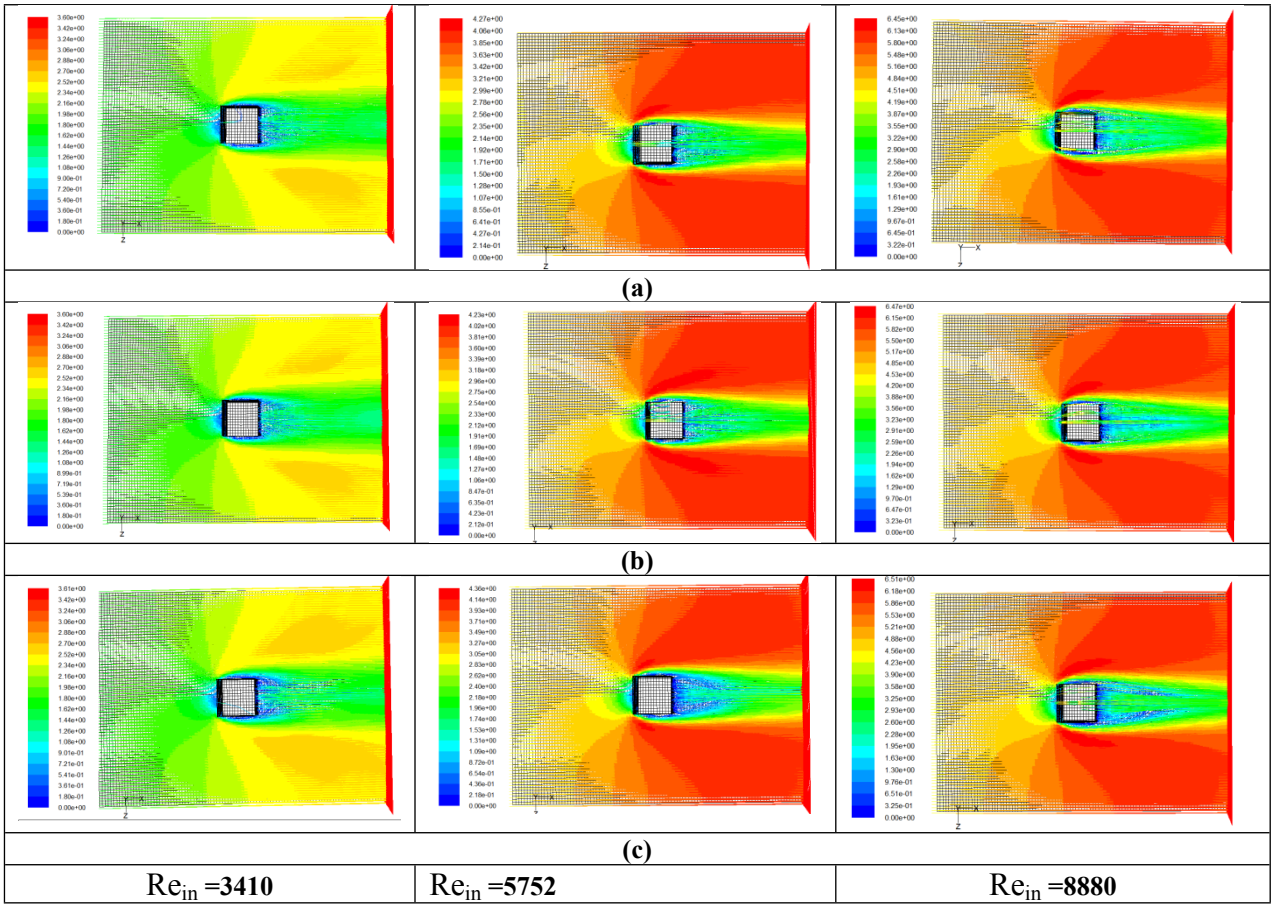

Figure IV.21: Streamlines for different air inlet Reynolds number at Re_j=1705: a-Regular cube,b-V-shaped mounted inside the cube with (P=-0.2),c-V-shaped mounted outside the cube with (P=0.2)

I.21.3.2.4 Velocity profiles

With "down 0.2" denoting the internal V-groove configuration and "up 0.2" denoting the external V-groove configuration, Figure IV.22 shows velocity evolution profiles for three configurations at constant jet Reynolds number (Rej=1705) across a range of inlet Reynolds numbers (Rein = 3410, 5752, and 8880). While both V-groove configurations exhibit initial flow acceleration effects near the groove regions, all configurations exhibit relatively modest velocity variations at lower Reynolds numbers (Rein = 3410), with the regular cube displaying conventional velocity profiles. The velocity profiles become more noticeable with stronger acceleration zones as the Reynolds number rises to 5752. This is especially noticeable in the external V-groove configuration, which exhibits increased velocity amplification because of flow channeling effects surrounding the external groove geometry. At the highest Reynolds

number (Re_{in} =8880), the external V-groove configuration consistently exhibits the most significant velocity enhancement and flow acceleration compared to the regular cube and internal V-groove, demonstrating superior flow mixing and convective heat transfer augmentation. The progressive velocity intensification with increasing crossflow Reynolds number confirms that the external V-groove geometry provides optimal flow field modification, creating enhanced velocity gradients and mixing that directly correlate with its superior thermal performance for cooling the 75°C electronic component.

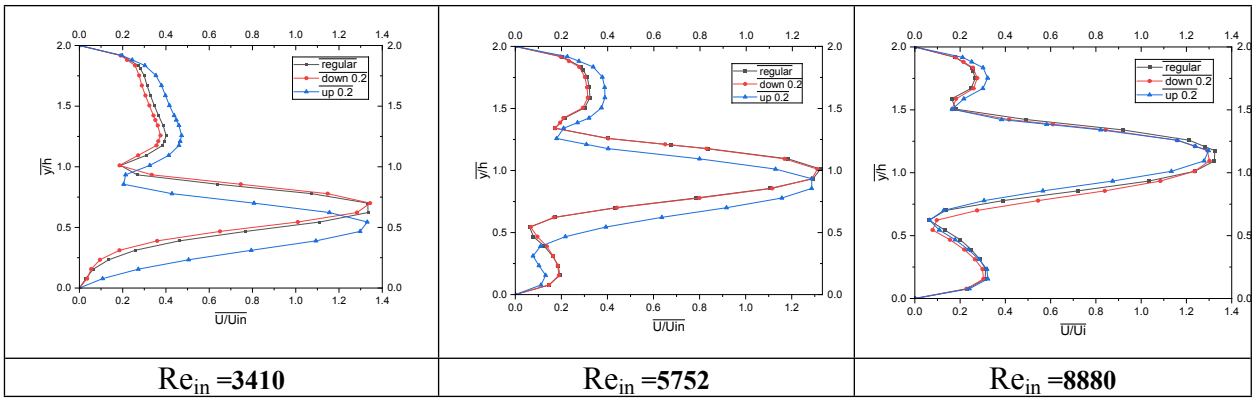

Re_{in} =3410	Re_{in} =5752	Re_{in} =8880

Figure IV.22: velocity evolution for different inlet Reynolds number at Re_j=1705: a-Regular cube,b-V-shaped mounted inside the cube with (P=-0.2), c-V-shaped mounted outside the cube with (P=0.2)

I.22 Conclusion

In comparison to regular and internal groove designs, the thorough numerical analysis unequivocally shows that external V-shaped groove configurations with maximum depth (P=0.2) offer better thermal management for electronic components operating at 75°C under all tested Reynolds number conditions (Rej=1705-5115, Reh=3410-8880). External grooves provide the most compact thermal wakes, the lowest peak temperatures, improved flow mixing, and the best convective heat transfer through superior flow field modifications, according to temperature contours, streamline analyses, and velocity profiles. The external V-groove is a reliable passive thermal management solution for high-performance electronic applications that need improved heat dissipation under a range of operating conditions. This is confirmed by the progressive performance improvement with increasing Reynolds numbers.

General Conclusion & recommandations

This numerical study effectively illustrated how V-shaped groove modifications can improve electronic component thermal management through a thorough computational fluid dynamics analysis using Fluent software with validation of the SST shear stress turbulence model. Internal and external V-shaped grooves mounted on the component's upper wall were the two main configurations that were systematically evaluated in the investigation. These configurations were tested under various operating conditions with different jet Reynolds numbers (Rej=1705, 3410, 5115) and inlet Reynolds numbers (Rein = 3410, 5752, 8880) as well as groove depths (P=0.05, 0.1, 0.15, 0.2). The findings unequivocally demonstrated that, out of all the tested Reynolds number combinations, the external V-shaped groove configuration with maximum depth (P=0.2) offers the best thermal performance and cools the electronic component at 75°C. In comparison to both the standard cube and internal groove configurations, the external groove geometry continuously showed improved heat dissipation through optimized flow field modifications, resulting in superior convective heat transfer mechanisms, improved flow mixing, and decreased thermal wake formation. The external V-groove maintains the lowest component temperatures, steepest temperature gradients, and most ordered flow structures, especially at higher crossflow Reynolds numbers where enhanced convective effects become dominant, according to temperature evolution profiles, streamline analyses, and velocity field distributions. These results show that external geometric modifications offer reliable and scalable cooling enhancement solutions for high-performance electronic systems that need effective heat dissipation under a range of operating conditions. They also offer important insights for real-world electronic thermal management applications.

Future Perspectives:

In order to improve thermal management performance, future research should examine advanced turbulence models like Large Eddy Simulation (LES) or Detached Eddy Simulation (DES) for more precise flow prediction, investigate nanofluid cooling with nanoparticles to increase thermal conductivity, validate numerical results experimentally, optimize groove

geometry parameters using multi-objective algorithms, and integrate hybrid cooling systems that combine passive grooves with active cooling technologies.

References

[1] J.-L. BATTAGLIA, A. KUSIAK, and J.-R. PUIGGALI, Introduction to Heat Transfer: Lessons and Solved Exercises, 2nd ed., Paris: Dunod, 2014.

[2] B. DEBICH, "Modeling, Simulation and Reliability of Phase Change Materials for Automotive and Aerospace Applications," PhD Thesis, Normandie University, 2021.

[3] National Laboratory of Metrology and Testing, "The Thermal Properties of Materials and Metrological References."

[4] Diane DUVAL, Thermal Fins, National Institute of Applied Sciences of Rouen, Department of Engineering Science and Technology, 2013.

[5] "Internal Combustion Engine Heat Transfer Outline," engr.colostate.edu.

[6] "Semiconductors," depts.washington.edu.

[7] J.-P. PETIT, "Thermal Dissipation in Electronic Systems: Thermal Characteristics of Components," Techniques de l'ingénieur, February 10, 2001.

[8] Millman,j.,and Halkias, C.C.1972 Electronic Devices and Circuits McGraw-Hill

[9] A. A. ALMUBARAK, "The Effects of Heat on Electronic Components," International Journal of Engineering Research and Application, pp. 52–57, May 2017.

[10] Pop, E, (2010). Energy dissipation and transport in nanoscale devices.Nano Reszarch,

3(3),147-169.

[11] Z. ZHANG, "Thermal Management of Power Electronic Components: Use of CVD Diamond," PhD Thesis, University of Toulouse, 2012.

[12] T. I. N. RASOLOFOMANANA, "Cooling of an Electronic Device Using a Thermal Fin," Master's Thesis, University of Antananarivo, 2016.

[13] L. MEYSENC, "Study of Integrated Micro-Heat Exchangers for the Cooling of Power Semiconductors," PhD Thesis, National Polytechnic Institute of Grenoble, 2013.

[14] H. LOUAHLIA and S. YON, “Thermal Dissipation in Electronic Components/Systems,” NAE-1214-01-R1A.

[15] M. TAWK, “Study and Implementation of a Cooling System for Power Electronics Based on the Movement of an Electrically Conductive Fluid,” PhD Thesis, University of Grenoble, 2011.

[16] Incropera, F. P., and Dewitt, D. P. 2002 Funddamentals of heat and masse transfer.

5th Edition, John Wiley and Sons

[17] A. LUU, “Methodology for Predicting Destructive Effects Due to the Natural Radiation Environment on Power MOSFETs and IGBTs,” PhD Thesis, University of Paul Sabatier - Toulouse III, 2009.

[18] Castro, I.P., and Robins, A.G. (1977). The flow around a surface-mounted cube in uniform and turbulent streams. Journal of Fluid Mechanics, 79, 307–335.

[19] Hussein, H.J., and Martinuzzi, R.J. (1996). Energy balance for turbulent flow around a surface-mounted cube placed in a channel. Physics of Fluids, 8, 764–780.

[20] Larousse, A., Martinuzzi, R.J., and Tropea, C. (1991). Flow around surface-mounted, three-dimensional obstacles. In Eighth Symposium on Turbulent Shear Flows, Vol. 1, Springer, Germany, pp. 1441–1446.

[21] Martinuzzi, R.J., and Tropea, C. (1993). The flow around surface-mounted, prismatic obstacles placed in a fully developed channel flow. Journal of Fluids Engineering, 115, 85–92.

[22] Moffat, R.J., and Ortega, A. (1986). Buoyancy Induced Forced Convection. AIAA/ASME Thermophysics and Heat Transfer Conference, Vol. 57, pp. 135–144, Boston, USA, June 1986.

[23] Ortega, A., and Moffat, R.J. (1985). Heat transfer from an array of simulated electronic components: Experimental results for free convection with and without a shrouding wall. In Heat Transfer in Electronic Equipment, ASME HTD, Vol. 48, pp. 5–15.

[24] Young, T.J., and Vafai, K. (1998). Convective cooling of a heated obstacle in a channel. International Journal of Heat and Mass Transfer, 41, 3131–3148.

[25] Kim, S.Y., Kang, B.H., and Hyun, J.M. (1998). Forced convective heat transfer from two heated blocks in pulsating channel flow. International Journal of Heat and Mass Transfer, 41(3), pp. 625–634.

[26] Kim, S.H., and Anand, N.K. (2000). Use of slots to enhance forced convective cooling between channels with surface-mounted heat sources. Numerical Heat Transfer, Part A, 38, pp. 1–21.

[27] Icoz, T., and Jaluria, Y. (2004). Design of cooling system for electronic equipment using both experimental and numerical inputs. ASME Journal of Electronic Packaging, 126, pp. 465–471.

[28] Hamouche, A., and Bessaih, R. (2009). Mixed convection air cooling of protruding heat sources in a horizontal channel. International Communications in Heat and Mass Transfer, 36, pp. 841–849.

[29] Amirouche, Y., & Bessaïh, R. (2010). Numerical simulation of laminar mixed convection air-cooling from an array of heated electronic components mounted in a vertical channel. In *Proceedings of the International Renewable Energy Congress (IREC)*, Sousse, Tunisia

[30] Niceno, B., Dronkers, A.D., and Hanjalic, K. (2002). Turbulent heat transfer from a multilayered wall-mounted cube matrix: a large eddy simulation. International Journal of Heat and Fluid Flow, 23, pp. 173–185.

[31] Meinders, E.R., and Hanjalic, K. (1999). Vortex structure and heat transfer in turbulent flow over a wall-mounted matrix of cubes. International Journal of Heat and Fluid Flow, 20, pp. 255–267.

[32] Sakakibara, J., Hishida, K., and Maeda, M. (1997). Vortex structure and heat transfer in the stagnation region of an impinging plane jet (simultaneous measurements of velocity and temperature fields by digital particle image velocimetry and laser-induced fluorescence). International Journal of Heat and Mass Transfer, 40, pp. 3163–3176.

[33] Masip Yunesky, Alejandro Rivas, Gorka S. Larraona, Raúl Anton, Juan Carlos Ramos, and Bahram Moshfegh (2012). Experimental study of the turbulent flow around a single wall-

mounted cube exposed to a cross-flow and an impinging jet. International Journal of Heat and Fluid Flow, 38, pp. 50–71.

[34] Rundström, D., and Moshfegh, B. (2009). Large-eddy simulation of an impinging jet in a crossflow on a heated wall-mounted cube. International Journal of Heat and Mass Transfer, 52, pp. 921–931.

[35] Smagorinsky. J, 1963. General circulation experimentwith the primitive equations I. the basicexperiment. Mon. WeatherRev .91 (3), pp. 99-164.

[36] Zhiyin. Y, 2015. Large-eddysimulation: Past, present and the future, Chinese Journal of Aeronautics, 28(1), pp. 11-24.

[37] Dellil Ahmed Zineddine, 2005. Investigation numérique du transfert de chaleur par convection forcée sur une paroi ondulée, thèse de doctorat d'état, Université des Sciences et de la Technologie d'Oran Mohamed BOUDIAF.

[38] Versteeg, H.K. & Malalasekera, W. (2007). An Introduction to Computational Fluid Dynamics: The Finite Volume Method. 2nd ed, Pearson Education Limited

[39] Jiyuan. T, Guan. H. Y, Chaoqun. L, 2007. ComputationalFluid Dynamics- A Practical Approach, pp. 65. ISBN: 978-0-7506-8563-4.

[40] Boussinesq. J, 1878. Essai sur la théorie des eaux courantes, Journal de mathématiques pures et appliquées, (4), pp. 335-376.

[41] Fluent. April 2009, ANSYS FLUENT 12.0 Theory Guide, ANSYS Inc., Sections 18.1.1 and 18.1.2

[42] Spalart. P. R, Allmaras, S. R, 1992. A one-equation turbulence model for aerodynamic flows, AIAA Paper 92-0439.

[43] Wilcox. D. C, 1993. Turbulence Modeling for CFD, DCW Industries, California.

[44] Menter. F. R, Kuntz. M, Langtry. R, 2003. Ten years of industrial experience with the SST turbulence model, in 'Proc. 4th Symposium on Turbulence, Heat and Mass Transfer. Begell House Inc., West Redding, pp. 625-632.

[45] Patankar. S. V, 1980. Numerical heat transfer and fluid flow, Mc-Graw Hill, New York.

[46] ATTOU Youcef, Etude numérique et thermique d'un écoulement turbulent dans un espace annulaire d'un rotor stator, Thèse de doctorat, Institut de Maintenance et de Sécurité Industrielle, Université d'Oran 2 Mohamed Ben Ahmed, 2019.